DRAFT

rec'd with ltr. dtd. 8/27/82

ONWI REPORT NO. ONWI/SUB/78/E511-01000-41

BNL Report No. 31921

The Role of <100> Edge Dislocations in Nucleating Radiation-Induced Colloid Particles in Sodium Chloride

by

L. J. Teutonico

September 1982

BATTELLE/ONWI SUBCONTRACT NO. E511-01000

BROOKHAVEN NATIONAL LABORATORY

UPTON, NEW YORK 11973

NOTICE

DRAFT

ONWI REPORT NO. ONWI/SUB/78/E511-01000-41

BNL Report No. 31921

The Role of <100> Edge Dislocations in Nucleating Radiation-Induced Colloid Particles in Sodium Chloride

by

L. J. Teutonico[1]

BATTELLE/ONWI SUBCONTRACT NO. E511-01000

BROOKHAVEN NATIONAL LABORATORY

UPTON, NEW YORK 11973

[1]Physics Department Consultant, now with the BNL Department of Nuclear Energy, Materials Technology Division.

This report was prepared by Brookhaven National Laboratory under Subcontract E511/01000 with Battelle Memorial Institute, Project Management Division, under Contract EY-76-0-06-1830 with the Department of Energy. The subcontract was administered by the Office of Nuclear Waste Isolation.

EXECUTIVE SUMMARY

It is now well established that the radiations from lightly shielded radioactive waste canisters embedded in rock salt will produce appreciable radiation damage, particularly sodium metal colloid particles, in the surrounding rock salt. Curves of colloid content vs. irradiation dose, measured for example at 150°C, can be described as classical nucleation and growth curves containing a pronounced induction period followed by a rapid growth regime. Colloid formation is either non-existent or negligible during the induction period, which extends up to 10^6 or 10^7 rad. At larger doses the colloid growth is very rapid and is described by $C(dose)^n$ relations. Extrapolating the currently available data, which extend to 2-4 x 10^8 rad, to the doses expected in actual repositories indicates that very large fractions of the rock salt adjacent to the planned canisters could be converted into sodium metal colloid particles and an equivalent amount of chlorine. The salt adjacent to planned canisters will receive doses in the 10^{10} to 2 x 10^{10} rad range in roughly 400 years. Between 0.1 and 10 percent of the salt is converted to colloidal sodium by 10^{10} rad and doses of 2 x 10^{10} rad could convert between 1 and 50 percent of the salt immediately adjacent to canisters to colloids in 200 to 600 years.

The plastic properties of rock salt are considered advantageous for waste disposal purposes. However, the radiation-induced colloid formation is strongly influenced by deforming the salt. The colloid growth induction period is reduced and the colloid growth rate increased by plastically deforming (straining) rock salt prior to irradiation. Also, the plastic properties play an important role in the mechanism for radiation damage formation in rock salt. The mechanism for colloid particle growth

is understood qualitatively but the mechanism for colloid particle nucleation is not at all understood. Since the nucleation step responsible for the induction period is strongly dependent on strain it is most likely that dislocations are involved in the nucleation process.

The analysis described in this report was undertaken to determine if the mobile <100> edge dislocations in NaCl have the requisite properties for nucleating radiation-induced colloid particles. Anisotropic elasticity theory is used to determine the strain field around the <100> dislocation and from this the "drift flow" describing the movement of defects to the dislocation is determined. In particular, the time required for defects to move to the dislocations is determined. It is found to be in good agreement with experimental data. From these results one can conclude that the <100> dislocation is a viable nucleating site for colloid particles in NaCl.

Underway is a similar calculation for the sessile (immobile) <111> edge dislocation in NaCl to determine if it also is a likely site for nucleating colloid particles. Although the calculation is not complete, the results available appear to be leading to the conclusion that the <111> dislocation is also a viable nucleation site and that the <100> and <111> dislocations are about equal in nucleating strength.

Additional calculations of this type would provide very useful information to determine enough of the nucleation process so as to be able to model it for calculations of colloid formation in actual repositories. Two things should be done. 1) Finish the <111> "drift flow" calculation. 2) Combine the <100> and <111> defect drift flow calculations with defect migration calculations that include defect diffusion.

To summarize, the <100> edge dislocation calculation is consistent with the observed data on radiation-induced sodium metal colloid formation in rock salt. Since it strongly supports the role of dislocations in nucleating radiation-induced colloids in rock salt, it is to be expected that other dislocation related properties of salt, e.g. strength, creep, etc. are influenced by radiation. The meager data available regarding strength support this conjecture, but data on the effects of radiation on creep are not available.

ABSTRACT

A theoretical program to investigate the role of dislocations in the nucleation of sodium colloids in irradiated rock salt has been outlined. As the first study in the investigation the interaction of radiation-produced defects with the <001> edge dislocation in rock salt, i.e. the edge dislocation in the principal slip system of NaCl, has been considered. The interaction potential between a symmetric defect and the <001> edge dislocation has been determined on the basis of anisotropic elasticity theory. The potential arises from the interaction between the long-range stress field of the dislocation and the displacements around the point defect. The corresponding flow lines, i.e. the lines along which the defects flow to the dislocation, have also been determined. In general, the flow lines are closed loops passing through the center of the dislocation. One of the novel features introduced by anisotropy is the possibility of open flow lines for certain elastic constant values. Along some of these open flow lines defects are attracted to the dislocation, whereas along others defects are repelled from the dislocation to a common plane.

The analysis of the migration kinetics of radiation-produced defects to the <001> edge dislocation has been carried out in the drift flow approximation in which flow to the dislocation is controlled only by the dislocation-defect interaction. In this approximation the edge dislocation is a sink for defects and a possible site for colloid nucleation. (The planar accumulation of defects that occurs along open flow lines for certain elastic constant values may represent a second dislocation-controlled mechanism for nucleation.) After the dislocation-defect inter-

action has been operating for some time, a region about the dislocation will have been depleted of defects. This region, referred to as the depletion zone, has been determined numerically for a range of elastic constant values which include those of unirradiated NaCl over the temperature range 24-700C. The defect flow, i.e. the number of defects reaching the dislocation per unit time, has also been determined numerically for this range of anisotropy.

The depletion time has been defined as the time required for the depletion zone to sweep out a specified area. Utilizing the elastic constants of unirradiated NaCl, the depletion times associated with the migration of F-centers to the <001> edge dislocation in rock salt have been computed for temperatures in the range 24-300C, the temperature range of interest for colloid formation in rock salt. The depletion process is strongly temperature-dependent. From the numerical results obtained for defect flow and depletion times it is concluded that the <001> edge dislocation is a viable site for colloid particle nucleation in rock salt.

I. INTRODUCTION

Recently completed radiation damage studies on natural rock salt, including samples from potential radioactive waste repository sites, demonstrate that the gamma-rays from the planned radioactive waste canisters will convert a large fraction of any rock salt immediately surrounding the canisters to sodium metal colloid particles. These studies show that curves of colloid concentration vs. irradiation time, or dose, follow classical nucleation and growth behavior. More explicitly, gamma-ray doses of 10^6 - 10^7 rad produce little or no colloid formation, i.e. a typical induction period is observed. Doses in excess of these values cause the colloid content to increase at a rapid rate given by expressions such as $C(\text{dose})^n$ or $C(\text{radiation time})^n$. Inserting experimentally determined values for the constants C and n in these relations it is estimated by extrapolation that a dose of 10^{10} rad could convert from approximately 0.1 to 10% of the natural rock salt samples studied to colloidal sodium metal. A dose of 2×10^{10} rad could convert between 1 and 50% of the samples studied to colloidal sodium metal. It is important to note that the colloid formation process is accelerated appreciably by straining samples prior to irradiation. Laboratory applied strains between 1 and 10% prior to irradiation reduce the induction period from 10^6 - 10^7 rad to a negligibly low dose (less than 10^3 rad). Preirradiation strains greater than approximately 10% do not produce any further detectable effects. It was established a number of years ago (Agullo-Lopez and Levy, 1964) that colloid formation in strained rock salt samples preferentially occurs on {110} slip planes. Electron microscope studies also indicate that both colloid formation and dislocation loops are formed during high dose rate

electron microscope irradiations (Hobbs, 1973). These studies clearly provide strong evidence to suggest that dislocations in the rock salt lattice play an important role in the nucleation of radiation-induced colloid particles.

To determine if dislocations in rock salt have the requisite properties for colloid nucleation sites, calculations were started to determine if radiation-induced defects in the rock salt lattice, particularly vacancies or F-centers, would be transported to dislocations at the temperatures where colloid nucleation occurs most readily. Two well-known processes are important for the migration of defects to dislocations. One of these is the diffusion of defects in the crystal lattice, a process which is strongly temperature dependent. The second process is the migration of defects due to the interaction between the defects and the strain, or lattice distortion, associated with dislocations. The overall migration of defects in the rock salt lattice can be considered as the superposition of the strain-related and normal diffusion processes. The strain-related processes cause certain defects to move towards the dislocations. Thus, the general problem can be regarded as a defect diffusion process taking place in the directionally oriented strain field of the dislocation. The general solution of this problem requires two steps. First, one calculates the strain field associated with the dislocation. Second, one combines the solution for the strain induced migration with the normal diffusion process. Most likely, the general solution is too complicated to obtain by analytic methods and one must resort to numerical solutions. However, as demonstrated below, analytical solutions can be obtained for the strain-related migration of defects to the <100> and

<111> edge dislocations in rock salt. The solution for the <100> edge dislocation is contained in this report and the solution for the <111> case will appear in a subsequent report.

Radiation damage in natural and synthetic rock salt: The information available in the literature on radiation damage and particularly radiation-induced colloid formation in natural and synthetic rock salt can be divided into two categories. The first category contains the information on radiation-induced and intrinsic defects in melt grown crystals of sodium chloride, and includes appreciable information on color centers. In the second category is specific information on radiation damage in natural and synthetic rock salt which, in one way or another, relats directly to the radioactive waste disposal program. Most of the information in the first category is contained in a number of books (Schulman and Compton, 1962; Fowler, 1968; Crawford and Slifkin, 1972; Markham, 1966; and Stoneham, 1975). A useful short survey of applicable information on color centers is contained in a recent encyclopedia article (Levy, 1981). It is very surprising that this extensive literature on color centers and defects, must of it dealing with alkali halides, contains almost no references to natural rock salt. Also, it contains very few references on radiation damage. color center and colloid formation in the alkali halides, and more specifically sodium chloride, above room temperature.

Although it has been known for many years that radiation produces colloid particles in the alkali halides, it is likely that the first indication that it might be of importance for radioactive waste disposal in natural rock salt appeared in the Lyons, KS, studies of Bradshaw and McLain (1971). Rock salt which had been irradiated at Lyons exhibited considera-

ble radiation damage. It was hard, brittle and almost black in color, indicating that it contained appreciable quantities of colloidal sodium.

More recent studies using electron microscope techniques on melt grown NaCl crystals made at Harwell show that the microscope beam irradiation introduced colloid particles and that colloid formation was accompanied by dislocation climb (Hobbs, 1973; Hobbs, Hughes and Pooley, 1973; Hobbs, 1975). This work also led to the conclusion that the colloid formation was strongly temperature dependent and that maximum colloid formation occurred at roughly 150°C. In an attempt to explain the results of Hobbs et al., Jain and Lidiard (1977) developed a theory for radiation-induced colloid formation in sodium chloride. In many respects this theory provides a qualitative understanding of radiation-induced colloid formation in NaCl. However, in some important respects, both qualitatively and quantitatively, the theory is not in accord with recent measurements. Most importantly, the theory is based on the assumption that the nucleation processes occur so fast it is unlikely they could be observed, i.e. the predicted induction period should be much shorter than is actually measured. Clearly the induction period plays an important role in colloid formation in natural rock salt. As mentioned above, a significantly long induction period in unstrained samples can be shortened by straining samples prior to irradiation, and the induction process appears to be related in some manner, the precise nature of which is to be determined, to the presence of dislocations in the crystal lattice.

In the past few years, radiation damage in both natural and synthetic rock salt has been intensively studied by a small group at Brookhaven National Laboratory. The principal experimental results, very

briefly sketched in the preceding paragraphs, have been outlined in a recent review article (Levy et al., 1981). Preliminary reports describing some of these results have been published previously (Swyler et al., 1979; 1980; Klaffky et al., 1979; Levy et al., 1980; 1981; 1982; 1983; Loman et al., 1981). Details on these radiation damage studies in natural and synthetic rock salt are included in reports, submitted or in preparation, for the Office of Nuclear Waste Isolation (ONWI). These include: 1) radiation damage in synthetic melt grown NaCl between 100 and 300 C (Swyler et al., 1982). 2) properties of the radiation-induced colloid particles in natural and synthetic rock salt (Klaffky et al., 1982). 3) heat-induced colloid formation in previously irradiated natural and synthetic rock salt (Elgort et al., 1982) and 4) thermoluminescence of irradiated natural and synthetic rock salt (Skinner et al., 1982).

To recapitulate, as described above, the available radiation damage information on synthetic and natural rock salt indicates that appreciable quantities of sodium metal colloid particles are introduced when samples are exposed to gamma-ray irradiation. Furthermore, curves of colloid concentration vs. dose are described by classical nucleation and growth curves with pronounced induction periods. The existence of the induction period demands that colloid growth is preceded by a pronounced nucleation stage. In turn, to understand this process to a reasonable degree, one must determine the nature of the nucleation process. Inasmuch as the nucleation stage depends markedly on the strain state of the material, it is likely that dislocations act as sites for colloid particle nuclei. To determine if dislocations are reasonable nucleation sites, the calculations described below have been undertaken. Specifically, they have been

designed to determine if the dislocation-defect interaction is strong enough for dislocations to be nucleation sites for colloid particle formation.

II. OUTLINE OF METHOD

The analysis of the kinetics of migration of point defects to a dislocation proceeds in three steps.

1) Determine the interaction energy between the defect and the dislocation.

2) Determine the lines of flow along which the defects move to the dislocation.

3) Determine the number of defects that migrate to the dislocation as a function of time.

Each of these steps is discussed in turn.

A. Interaction Energy: Of the various types of interactions (electrical, chemical, and elastic) between a point defect and a dislocation, the elastic interaction is usually the most important (Bullough and Newman, 1970). It arises from the interaction between the long-range stress field of the dislocation and the atomic displacements around a point defect. The analytic form of this interaction is usually deduced from a continuum model in which the crystalline body is replaced by an anisotropic elastic medium described by the elastic constants of the crystal. The dislocation is simulated by the appropriate elastic stress field, usually referred to as a Volterra dislocation. A point defect is similarly simulated by an elastic inclusion. The latter is introduced by forcing an elastic sphere of radius $r_0(1+\epsilon)$ into a spherical hole of radius r_0 in the elastic continuum. The interaction energy U between the inclusion and the stress field σ_{ij} of the dislocation is given by

$$U = P\cdot(\Delta V) = -(4/3)\,\pi\epsilon r_0^{\,3}(\sigma_{11}+\sigma_{22}+\sigma_{33}) \qquad (1)$$

where $\Delta V = 4\pi\epsilon r_0^3$ is the change in volume of the sphere, and $P = -(1/3)(\sigma_{11} + \sigma_{22} + \sigma_{33})$ is the hydrostatic pressure of the stress field (Cottrell, 1953). In the Appendix it is shown that for cubic crystals one can write, regardless of the dislocation orientation,

$$P = -B\Delta \tag{2}$$

where

$$B = \frac{1}{3}(c_{11} + 2c_{12}) \tag{3}$$

is the bulk modulus, and

$$\Delta = \epsilon_{11} + \epsilon_{22} + \epsilon_{33} \tag{4}$$

is the dilatational field of the dislocation. In the above expressions the c_{ij} are the elastic constants and the ϵ_{ij} are the strain field components of the dislocation. Equation (1) can be rewritten as

$$U = -4\pi\epsilon r_0^3 B\Delta \quad . \tag{5}$$

Therefore a determination of the elastic interaction between a point defect and a dislocation in a cubic crystal reduces to a determination of the dilatational field of the dislocation.

The strain field of a dislocation varies inversely with distance from the center of the dislocation. Hence, taking (R,ϕ) to be polar coordinates about an infinitely long dislocation, the interaction energy U will have the general form

$$U = E\frac{D(\phi)}{R/b} \tag{6}$$

where b is the magnitude of the Burgers (slip) vector of the dislocation, E is a constant with units of energy, and $D(\phi)$ is a dimensionless function of angle.

B. Flow Lines: A point defect in a dislocation stress field experiences a force, proportional to the gradient of the interaction, which attracts it to the dislocation. In general this force is non-central since U is a function of angle as well as distance from the dislocation. At any point the gradient of U is normal to the local equipotential lines. Hence the flow lines along which the defects move are the family of curves orthogonal to the equipotentials of the point defect-dislocation interaction. From eq. (6), the general form of this interaction, it can be shown that the flow lines have the form

$$R/b = \exp\left\{-\int \frac{D(\phi)}{D'(\phi)}\, d\phi\right\} \tag{7}$$

C. Defect Flow: The movement of defects along the flow lines solely as a result of the defect-dislocation interaction is referred to as drift flow. The drift flow is superimposed on any defect migration associated with thermal diffusion processes. When both processes are operating the defect migration kinetics depend upon the precise nature of the interaction potential U and any defect concentration gradients which are present. The concentration of defects, c, must satisfy the following equation of continuity

$$\frac{1}{D_f}\frac{\partial c}{\partial t} = \nabla^2 c + \frac{\nabla\cdot(c\nabla U)}{kT} \tag{8}$$

where D_f is the diffusion coefficient at temperature T, k is Boltzmann's constant, and U the dislocation-defect interaction energy (Bullough and Newman, 1970). If the initial defect concentration is c_0 at time zero, then the migration of defects to a nearby dislocation is governed by eq. (8) and the appropriate boundary conditions.

The calculations described here will be concerned with the intrinsic properties of dislocations which would make them likely sites for radiation-induced colloid nucleation, and also with determining which of the various possible dislocations are the more probable nucleation sites. Only drift flow solutions of eq. (8) will be considered, i.e. the cases in which drift flow predominates and thermal diffusion is totally neglected ($\nabla^2 c = 0$). In the paper by Bullough and Newman (1970) evidence is presented indicating that the initial accumulation rate for defects at a dislocation is due almost entirely to drift flow, i.e. that flow due to concentration gradients is negligible during the initial stages of defect flow.

For each dislocation considered the calculations will determine the flow of defects to dislocations as a function of time, N(t). Because of the dislocation-defect interaction, the defects move along the flow lines until they reach the center of the dislocation which, in the drift flow approximation, is an ideal sink. In other words, this corresponds to putting c = 0 at the center of the dislocation.

After the defect-dislocation interaction has been operating for some time and if new defects are not being introduced, a well-defined area surrounding the dislocation will have been depleted of defects. This area is called the depletion zone. The determination of the defect flow is

equivalent to determining the depletion zone area, weighted by the defect concentration, as a function of time, or

$$N(t) = 1/2 \int_0^{2\pi} c \cdot R_0^2 \, d\phi \tag{9}$$

where $R = R_0(\phi)$ represents the depletion zone boundary.

III. RESULTS FOR THE <001> EDGE DISLOCATION

The principal slip system in rock salt is $\langle 110 \rangle \{1\bar{1}0\}$, i.e. dislocations prefer to glide on $\{1\bar{1}0\}$ planes in <110> directions. In general, dislocation-point defect interactions are greatest for edge dislocations. Hence the first dislocation to be considered as a possible colloidal nucleation site is the edge dislocation in the principal slip system of rock salt. This dislocation lies along an <001> direction.

A. Interaction Energy: The specific slip system considered is that in which the edge dislocation lies along the $[001]$ direction and has a Burgers vector parallel to the $[1\bar{1}0]$ direction in the (110) plane. The dilatational field Δ of this edge dislocation (Chang, 1962; Chou, 1963), referred to the set of axes y_i where $y_1 \| [1\bar{1}0]$, $y_2 \| [110]$, $y_3 \| [001]$, is

$$\Delta = -\frac{bKy_2}{2\pi} \frac{(2+H)y_1^2+2y_2^2}{y_1^4+(2+H)y_1^2y_2^2+y_2^4} . \qquad (10)$$

This can be rewritten in polar coordinates (R,ϕ) as

$$\Delta = -\frac{bK\sin\phi}{2\pi R} \frac{(2+H\cos^2\phi)}{(1+H\sin^2\phi\cos^2\phi)} \qquad (11)$$

where ϕ is the angle about the dislocation line measured from the slip plane. In these expressions K is a measure of the dilatational field strength and is given by

$$K = \left[\frac{c_{44}(c_{11}-c_{12})}{c_{11}(c_{11}+c_{12}+2c_{44})}\right]^{1/2} . \qquad (12)$$

H is a measure of the anisotropy of the elastic continuum and is given by

$$H = -\frac{4(c_{11}+c_{12})(c_{11}-c_{12}-2c_{44})}{(c_{11}-c_{12})(c_{11}+c_{12}+2c_{44})} \tag{13}$$

where c_{11}, c_{12}, and c_{44} are the elastic constants of the cubic material.

The condition of crystal stability imposes certain restrictions on the range of values of the elastic constants. These restrictions, called the elastic stability criteria, are determined by imposing the condition that the energy density of a deformed elastic body be positive-definite for all stress and strain values. For a cubic crystal the elastic stability criteria are $c_{11}-c_{12} > 0$, $c_{11}+2c_{12} > 0$, $c_{11} > 0$, $c_{44} > 0$. From the latter the ranges of values of the dilatational field strength K and the anisotropy parameter H are found to be $0 < K < \sqrt{3}/2$ and $-4 < H < \infty$. In the singular case of elastic isotropy H is equal to zero, and the expression for K reduces to $(1-2\nu)/2(1-\nu)$, where ν is Poisson's ratio.

The elastic constants of unirradiated NaCl have been reported for the temperature range 24C-700C (Hart, 1968). The values of H and K in the same temperature range are shown in Fig. 1, having been computed from eqs. (12) and (13), respectively, using the reported values of c_{11}, c_{12}, and c_{44}. The values of H are in the interval $-1 < H < +1$ whereas the K values vary only between 0.31 and 0.36.

At the high irradiation levels for which the present calculations are applicable, one expects considerable changes in the elastic constants with concomitant variations in the H and K values. It is expected that irradiation will increase the value of each elastic constant. For computational purposes this can be regarded as lowering the crystal temperature. Whether the quantities H and K increase or decrease, and to what extent, will depend on the variation of each elastic constant with

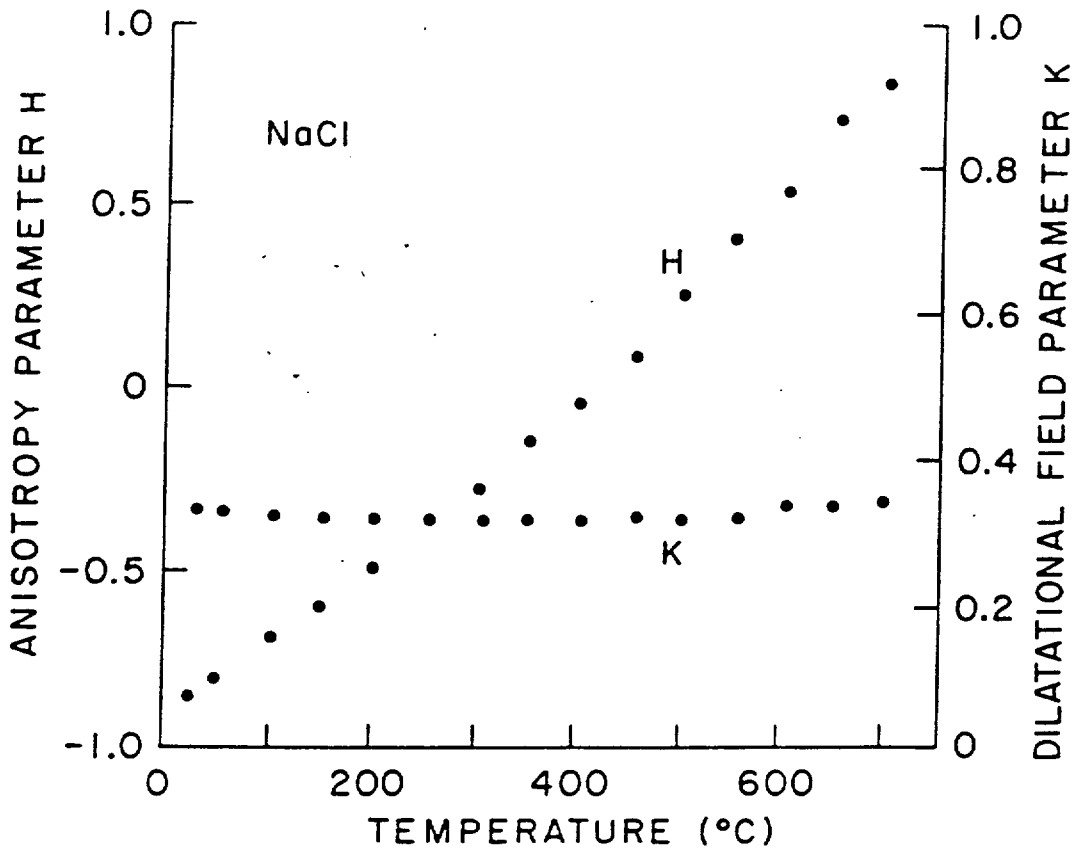

Fig. 1. The anisotropy parameter H and the dilatational field strength parameter K as a function of temperature in unirradiated NaCl. These parameters were computed from equations (12) and (13) in the text using the elastic constant data from Hart (1968).

irradiation. Since the radiation-induced elastic constant changes are not known, the theoretical analysis will be carried out for arbitrary elastic constant values. Consequently the analysis will apply to other cubic materials, such as KCl.

The principal features of the dilatational field Δ, eq. (10) or (11), are as follows. For values of the anisotropy parameter H in the range $-2 < H < \infty$, the dilatational field is negative above the slip plane of the edge dislocation, positive below the slip plane, and zero on the slip plane. In other words the region above the slip plane which has to accommodate the extra plane of the edge dislocation is in a state of compression, and conversely the region below the slip plane is in a state of tension. For values of H in the range $-4 < H < -2$ there are regions of tension and compression both above and below the slip plane, the additional zeroes in the dilatational field occurring at angles ϕ_0 given by $\cos^2 \phi_0 = -2/H$. The values of the dilatational field Δ at angles of 0°, 45°, and 90° from the slip plane are independent of H.

Putting the expression for the dilatation Δ, eq. (11), into eq. (5), the dislocation-point defect interaction energy for the <001> edge dislocation becomes

$$U = \frac{E}{\rho} \frac{\sin \phi \ (1+\alpha \cos 2\phi)}{(1-\alpha \cos^2 2\phi)} \tag{14}$$

where

$$\rho = R/b \tag{15}$$

$$E = 4\varepsilon r_0^3 \, KB \tag{16}$$

and

$$\alpha = H/(4+H) \qquad -\infty < \alpha < 1 \quad . \tag{17}$$

B. Flow Lines: The equipotential lines form a family of curves passing through the center of the dislocation. The change in U from one curve to the next produces a force on each defect which causes it to acquire a drift velocity in the direction perpendicular to the local equipotential line. Thus, the flow lines along which the defects move are given by the family of curves orthogonal to the set of equipotentials, as represented in eq. (7). Utilizing the interaction potential, eq. (14), for the <001> edge dislocation, the latter can be written

$$R/b = \exp\left\{\int \frac{(1+\alpha x)(1-\alpha x^2)}{2(x+1)f(x,\alpha)}\, dx\right\} \tag{18}$$

where

$$x = \cos 2\phi \tag{19}$$

and

$$f(x,\alpha) \equiv \alpha^2 x^3 + \alpha(3-2\alpha)x^2 - \alpha x + (1-2\alpha). \tag{20}$$

Analytic Form of the Flow Lines: The integration indicated in (18) can always be carried out, i.e. an analytic solution for the flow lines can be obtained. However the particular analytic form of the flow lines depends on the nature of the roots x_1, x_2, x_3 of $f(x,\alpha) = 0$. These roots are shown as functions of H in Fig. 2. There are three real roots unless H is in the interval $0 < H < H_0$, where H_0 is that value of H for which two of the real roots are equal, namely

$$H_0 \equiv \frac{(292823 + 12096\sqrt{497})^{1/3} + (292823 - 12096\sqrt{497})^{1/3} - 25}{24} \approx 3.5855. \quad (21)$$

The root x_1 is taken to be always real. In the range $0 < H < H_0$, the roots x_2 and x_3 are given by $x_{2,3} = k \pm i\ell$ (k, ℓ real). The values of k and ℓ are plotted in Fig. 2 for the range of H values $0 < H < H_0$.

In addition to the two general cases corresponding to one or three real roots of the polynomial $f(x,\alpha)$, the integration in eq. (18) must be carried out separately for the values $H = 0$, H_0, and -1. For the latter two H values the denominator of the integrand in (18) has multiple roots, whereas, for $H = 0$, $f(x,0)$ is equal to unity. The analytic expressions for the flow lines are

$$R/b = \begin{cases} C|x+1|^{\frac{1}{2(H+1)}} |x-x_1|^{p_1} |x-x_2|^{p_2} |x-x_3|^{p_3} & \begin{pmatrix} -4<H<-1 \\ -1<H<0 \\ H_0<H<\infty \end{pmatrix} \quad (22a) \\ C|x+1|^{\frac{1}{2(H+1)}} |x-x_1|^{p_1} \left[(x-k)^2+\ell^2\right]^q \exp\left\{r \tan^{-1}\left(\frac{x-k}{\ell}\right)\right\} & 0<H<H_0 \quad (22b) \\ C|x+1|^{\frac{1}{2(H_0+1)}} |x-x_1|^{p_1} |x-x_0|^{\lambda_0} \exp\{\mu_0/(x_0-x)\} & H=H_0 \quad (22c) \\ C|x+1|^{-1/14} |x-x_1|^{p_1} |x-x_2|^{p_2} \exp\{-2/7(x+1)\} & H=-1 \quad (22d) \\ C|x+1|^{1/2} & H=0 \quad (22e) \end{cases}$$

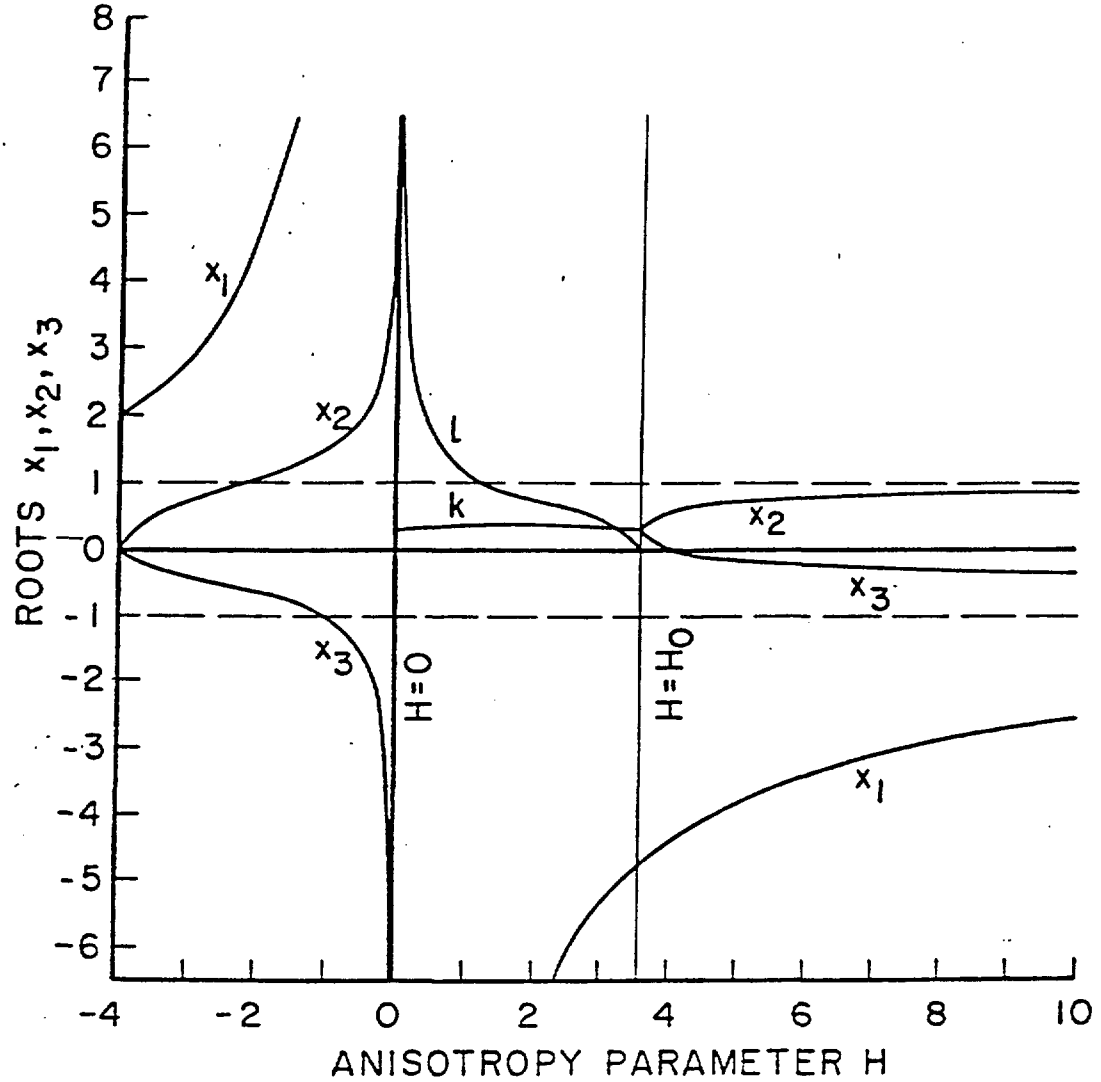

Fig. 2. The roots x_1, x_2, x_3 of the polynomial $f(x,\alpha)$, Eq. (20) in the text, as a function of the anisotropy parameter H. In the interval $0<H<H_o$, $x_{2,3} = k \pm i\ell$ (k,ℓ real). Also, as $H\to\infty$, $x_1\to-1$, $x_2\to+1$, $x_3\to-1$.

where, in each expression, C is a parameter specifying the different curves in each family of flow lines. The values of the other parameters are as follows: In eq. (22a) the exponents p_1, p_2, p_3 are given by

$$p_1 = \frac{hx_1^2+fx_1+d}{(x_1-x_2)(x_3-x_1)} \; ; \; p_2 = \frac{hx_2^2+fx_2+d}{(x_1-x_2)(x_2-x_3)} \; ; \; p_3 \; \frac{hx_3^2+fx_3+d}{(x_2-x_3)(x_3-x_1)} \tag{23}$$

where

$$h = \frac{(H+2)}{2(H+1)} \; , \; f = \frac{2(H+4)}{H(H+1)} \; , \; d = \frac{-(H+6)(H+4)}{2H(H+1)} \tag{24}$$

Similarly, p_1, q, r in eq. (22b) are given by

$$p_1 = \frac{(hx_1^2+fx_1+d)}{\{(x_1-k)^2+\ell^2\}}$$

$$q = \frac{-(p_1+h)}{2} \tag{25}$$

$$r = \frac{2q(x_1-k)-(2hk+f)}{\ell}$$

where h, f, and d are again given by (24). With ω defined as

$$\omega \equiv (H_0^2+9H_0+36)^{1/2} \simeq 9.007 \tag{26}$$

the parameters in the flow line solution for $H = H_o$, eq. (22c), are given by

$$x_1 = \frac{-(12+H_0)+4\omega}{3H_0} \simeq -4.798$$

$$x_2 = x_3 \equiv x_0 = \frac{2\omega-(12+H_0)}{3H_0} \simeq 0.2257 \tag{27}$$

$$p_1 = -\frac{3(5H_0+12)(5H_0+36)+8\omega H_0(H_0+8)}{72\omega^2(H_0+1)} \simeq -0.2925$$

$$\lambda_0 = \frac{H_0\{3(5H_0^2+33H_0+84)-2\ (H_0+8)\}}{18\omega^2(H_0+1)} \simeq -0.3165$$

$$\mu_0 = \frac{(H_0+8)(H_0+\omega)}{9\omega(H_0+1)} \simeq 0.3925$$

Lastly, in the expression for H = -1, eq. (22d),

$$x_{1,2} = 6 \pm \sqrt{21} \simeq 10.58,\ 1.417$$

(28)

$$p_{1,2} = \frac{-3}{14}\left(1 \pm \sqrt{3/7}\right) \simeq -0.3546,\ \ -0.0740$$

The quantities p_1, p_2, p_3, q, r are plotted in Fig. 3 as functions of H. It should be noted that, whereas p_1 is negative for all values of H, the exponents p_2 and p_3 can be either positive or negative, depending on H value.

Properties of the Flow Line Solutions: The nature of the flow lines can be ascertained by considering the various factors in eq. (22). For example, the term $|x+1| = 0$ at $\phi = \pm\pi/2$. The term $|x-x_1| > 0$, since $|x_1| > 1$ for all H. The term $|x-x_2|$ will be zero at certain values of x, i.e. at certain angles ϕ_2, for both $-4 < H < -2$ and $H_0 < H < \infty$, since $|x_2| < 1$ for these values of H (see Fig. 2). Similarly the term $|x-x_3| = 0$ at certain angles ϕ_3 for H values in the ranges $-4 < H < -1$ and $H_0 < H < \infty$. The angles ϕ_2, ϕ_3 are defined by

$$\phi_{2,3} = \frac{1}{2}\cos^{-1} x_{2,3} \qquad (29)$$

For each value of x_2 or x_3 there are obviously four angles that satisfy (29). The positive acute angle is shown as a function of H in Fig. 4. Whether any of the terms $|x+1|$, $|x-x_2|$, $|x-x_3|$ represents a zero or infinity in the flow line solution (22) will depend on the sign of its respective exponent. Using eg. (22) and the results shown in Fig. 3, it is found that there are two general types of flow lines, depending on whether or not H lies in the interval $-1 \leq H < H_0$.

(1) H values in the interval $-1 \leq H < H_0$:

In this case the flow lines are closed curves consisting of two symmetric sets. One set of curves lies on either side of the dislocation and passes through the center of the dislocation. In this H range all of the loops are closed, but their shape depends on the value of H.

(2) H values not in the interval $-1 \leq H < H_0$:

Within an angle ψ on either side of the slip plane there are closed flow lines on each side of the dislocation which pass through the center of the dislocation. ψ is the acute angle ϕ_2 for $H_0 < H < \infty$, and the acute angle ϕ_3 for $-4 < H < -1$, where ϕ_2 and ϕ_3 are defined in eq. (29) and shown in Fig. 4. In fact, for $-4 < H < -2$, there are three closed loops on either side of the dislocation. Outside of the region defined by the angle ψ the flow lines do not close. This follows from the fact that R, in eq. (22), becomes infinite at certain angles. In the range $-4 < H < -1$, R becomes infinite at $\phi = \pm\pi/2$, and for $H_0 < H < \infty$, R becomes infinite at the four angles $\phi = \pm\phi_3, \pi\pm\phi_3$, where ϕ_3 is the acute angle defined by (29) and shown in Fig. 4.

The possibility that open flow lines might occur is a unique feature introduced by crystal anisotropy. It should not be regarded as something

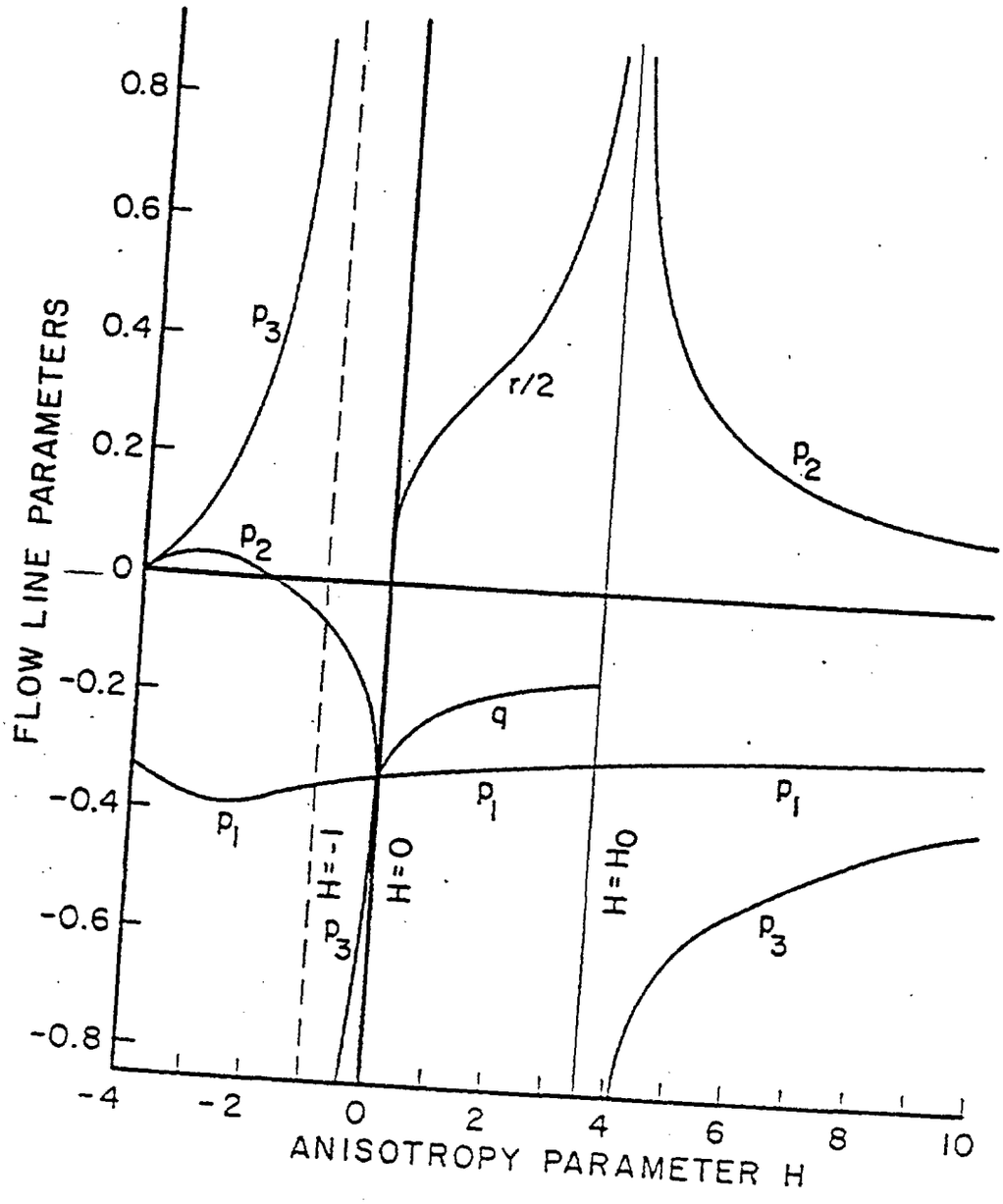

Fig. 3. The parameters p_1, p_2, p_3, q,r in the flow line solution, Eq. (22) in the text, as a function of the anisotropy parameter H. As $H\to\infty$, $p_1\to -1/4$, $p_2\to 0$, $p_3\to -1/4$.

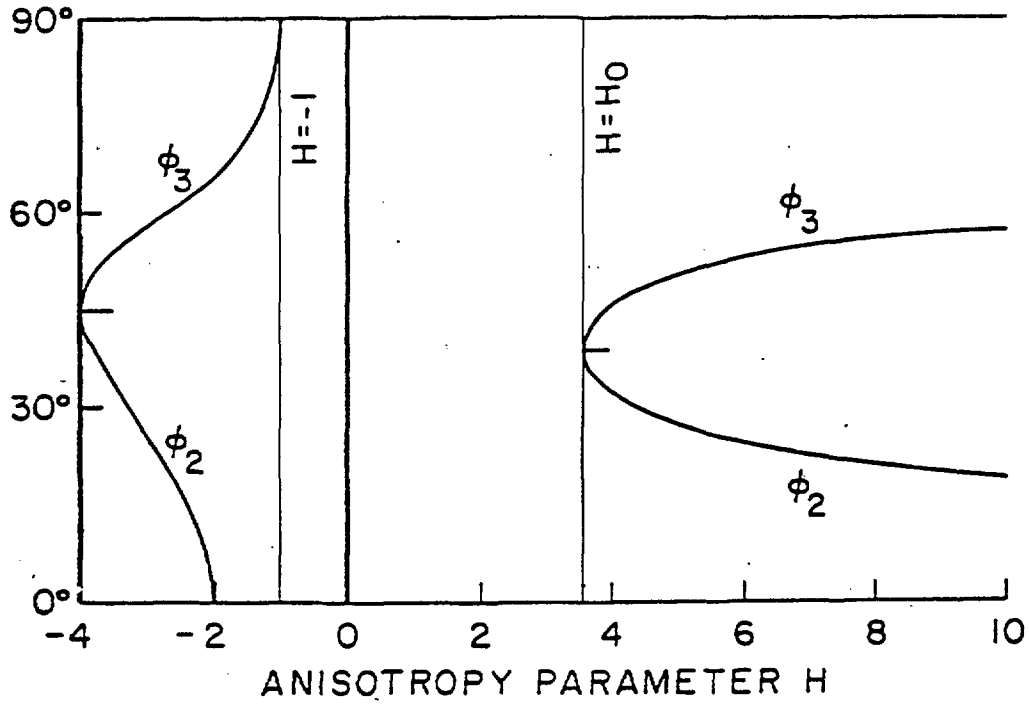

Fig. 4. The acute angles ϕ_2 and ϕ_3, Eq. (29) in the text, plotted as a function of the anisotropy parameter H. The angle ϕ_2 is defined only for values of H outside the interval $-2<H<H_o$. There is a zero in the flow line solution at the angle ϕ_2. The angle ϕ_3 is defined only for H values outside the interval $-1<H<H_o$. For $-4<H\leq 1$ there is a zero in the flow line solution at the angle ϕ_3, whereas for $H_o<H<\infty$ the flow line diverges to infinity at the angle ϕ_3. Also, as $H\to\infty$, $\phi_2\to 0$, $\phi_3\to 90°$.

of only mathematical interest. Recall that the H value of unirradiated NaCl is -0.85 at room temperature. The change in elastic constants induced by radiation damage can be regarded as the equivalent of going to lower temperatures. Hence values of $H < -1$ in highly irradiated rock salt appear to be likely. Also, note that H values outside the interval $-1 \leq H < H_0$ can be found in other cubic crystals. For example, in the temperature range 24C-700C, H values for unirradiated KCl, calculated from the elastic constant data of Hart (1968), are in the interval $-2 < H < -0.7$. Similarly, for unirradiated LiF (Hart, 1977) H values over the temperature range 24C-650C are in the interval $2 < H < 5$.

Direction of Defect Flow: To determine the direction that defects flow along either open or closed flow lines one must consider the forces acting on the defect. These are given by

$$F_R = \frac{-\partial U}{\partial R}, \quad F_\phi = -\frac{1}{R}\frac{\partial U}{\partial \phi} \tag{30}$$

where U is the dislocation-defect interaction energy, and (R,ϕ) are polar coordinates about the dislocation line. With U given by eq. (14), these expressions become

$$F_R = \frac{Eb}{R^2}\frac{\sin\phi(1+\alpha x)}{(1-\alpha x^2)} \tag{31}$$

$$F_\phi = -\frac{Eb}{R^2}\frac{\cos\phi \cdot f(x,\alpha)}{(1-\alpha x^2)^2}$$

where $f(x,\alpha)$ is defined in eq. (20). Note that the force is purely radial only at $\phi = \pm\pi/2$, and at the angles $\phi = \phi_2, \phi_3$ defined in eq. (29). The force is purely tangential at $\phi = 0,\pi$ and, for $-4 < H < -2$, at angles given by $1/2 \cos^{-1}(-1/\alpha)$.

Effects of Anisotropy: Elastic anisotropy not only changes the flow line shape but also introduces novel features in the dislocation-defect interaction. For $H = 0$ the flow lines are circles. As H increases from zero the closed flow lines are elongated about the slip plane. At $H = H_0$ the closed flow lines are restricted to an angular zone within 45° of the slip plane. For larger values of H the angular zone for closed flow lines diminishes until it vanishes in the limit $H \to \infty$. As H decreases from zero, the flow lines are elongated normal to the slip plane. For H less than -1, the zone of closed flow lines diminishes. The closed flow lines are restricted to a zone within an angle Ω of the slip plane, where Ω is $\pi/2$ at $H = -1$ and decreases to $\pi/4$ as $H \to -4$.

All of the above features are illustrated in Figs. 5 and 6, which show both the equipotential lines and flow lines for H values of -3, -2, -1, 0, 1, 3, and 4. The directions of flow shown are for E positive, i.e. for $\varepsilon > 0$, which corresponds to defects which expand the elastic continuum. (For $\varepsilon < 0$, the directions of all arrows would be reversed). The plots for H = -1, 0, 1, and 3 show that all flow lines in the range $-1 \leq H < H_o$ are closed. Hence all defects, both those that expand or contract the elastic continum, will eventually migrate to the dislocation. The plots for H = -3, -2, and 4 show that outside the range $-1 \leq H < H_o$ both open and closed flow lines are obtained. More specifically, the closed flow lines represent the flow of defects to dislocations. For $\varepsilon > 0$ as shown, the

open flow lines in the lower half-plane do likewise but those in the upper half-plane do not. In other words there is a range of angles about the edge dislocation in the upper half-plane for which defects will not flow to the dislocation. (For $\epsilon < 0$, defects are attracted along open flow lines in the upper half-plane, and repelled along open flow lines in the lower half-plane.) The defects which are repelled from the dislocation are driven to a common plane. More exactly, in the continuum theory approximation, the defects approach this plane asymptotically. For $-4 < H < -1$ this plane is given by $\phi = \pi/2$, i.e. the half-plane perpendicular to the slip plane. For $H_0 < H < \infty$ the defects are driven to two half-planes above the slip plane which are symmetric about the dislocation and given by $\phi = \phi_3, \pi-\phi_3$, where ϕ_3 is the acute angle shown in Fig. 4.

This last feature, the existence of a plane to which the defects are repelled, is not readily apparent in Figs. 5d and 6d. To make it more evident the flow lines for $H = -3$ and 4 have been replotted in Fig. 7 on a much larger scale than that employed in Figs. 5d and 6d. For $H = -3$ the repelled defects accumulate on the plane given by $\phi = \pi/2$, which is the $(1\bar{1}0)$ plane. For $H = 4$ the defects are repelled to planes given by $\phi = 45°, 135°$, which correspond to the (010) and (100) planes, respectively. In general, the indices of the two planes to which the defects are repelled, for values of H in the interval $H_0 < H < \infty$, are given by $(\bar{1}V0)$, where $V = \tan(\pi/4 \pm \phi_3)$.

The flow of defects to the dislocation center, which is assumed to be a defect sink, and which occurs for all H values could be the basis for a mechanism for colloid nucleation in irradiated rock salt. In addition, the existence of planes on which defects could accumulate, which occurs

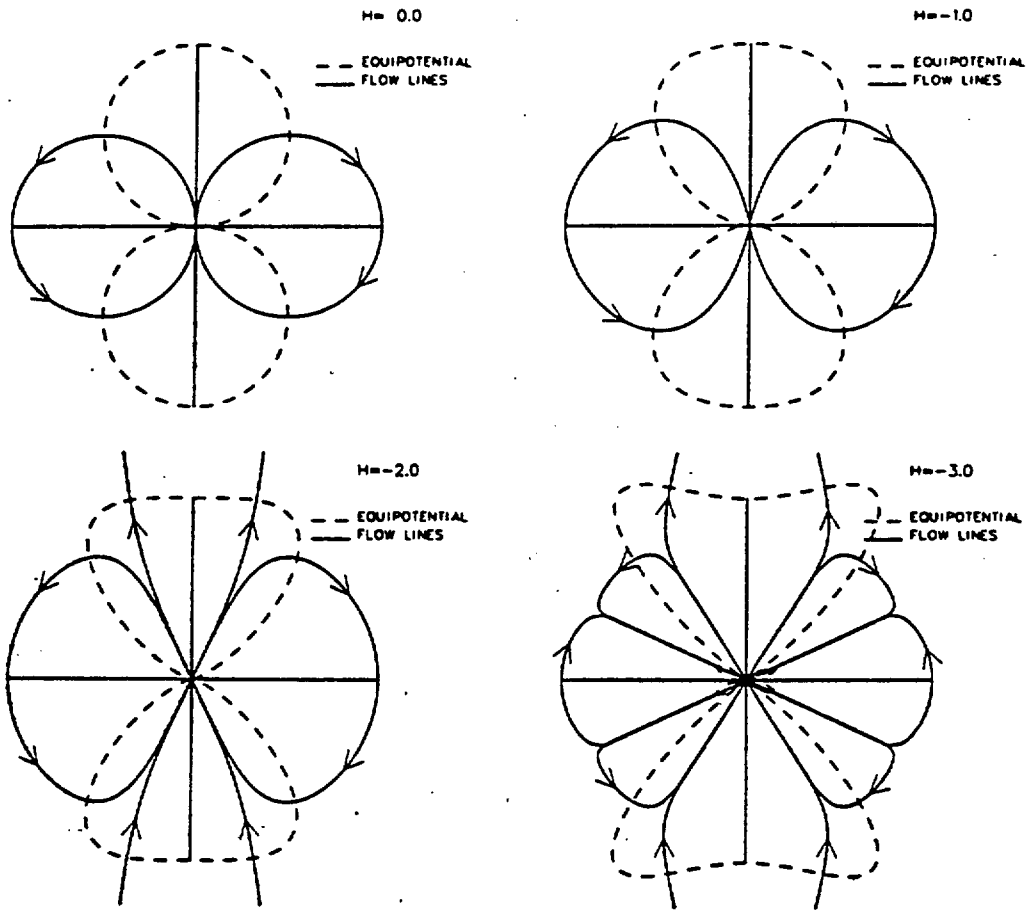

Fig. 5. Equipotentials and orthogonal flow lines for the drift of defects to an <001> edge dislocation for H values equal to (a) 0, (b) -1, (c) -2, and (d) -3. The arrows show the direction of flow for a defect which corresponds to a volume expansion. All closed flow lines are paths along which defects are attracted to the center of the dislocation. In those regions where open flow lines occur, only defects in the lower half plane are attracted to the dislocation.

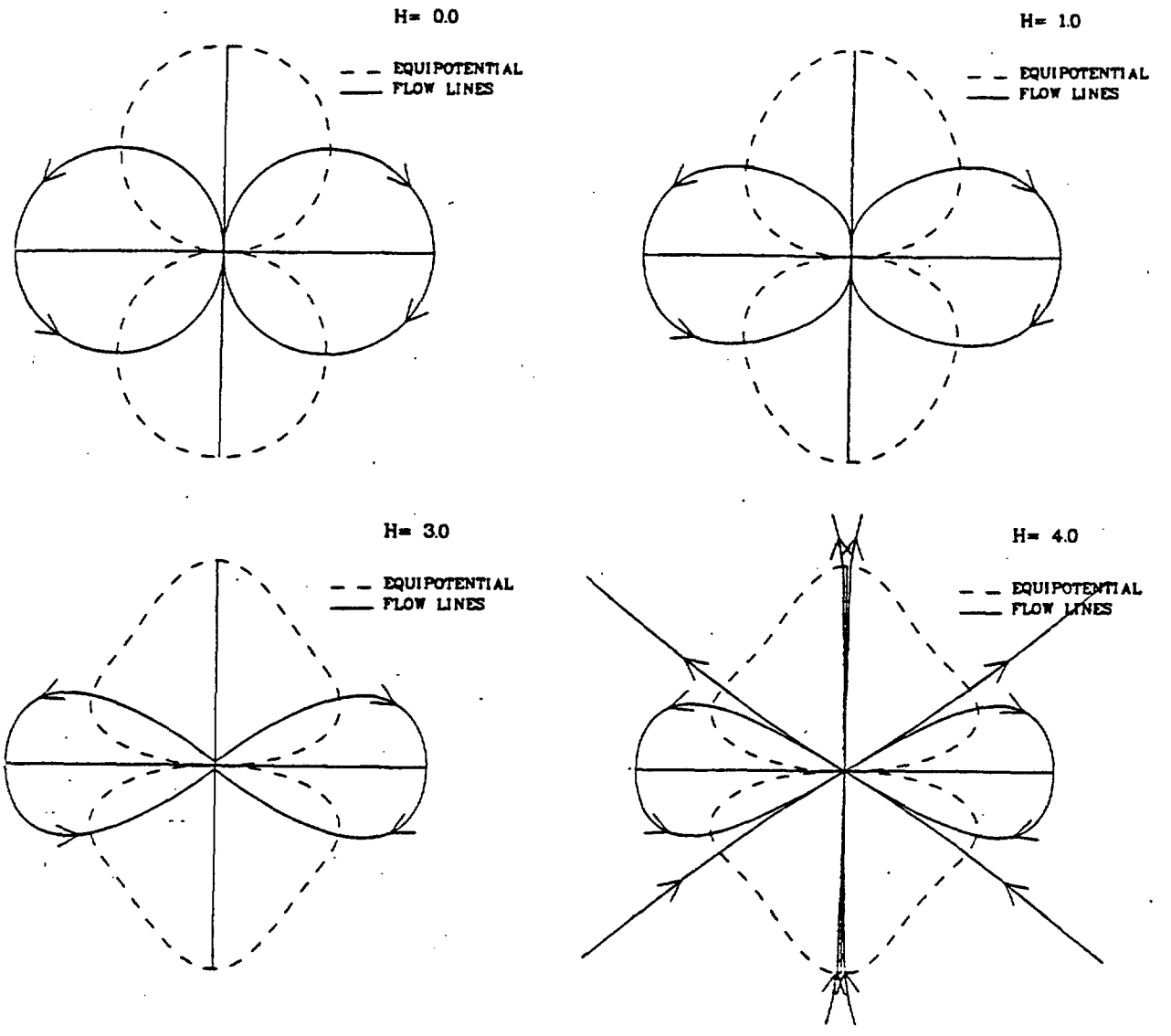

Fig. 6. Same as Fig. 5 for H values (a) 0, (b) 1, (c) 3, and (d) 4.

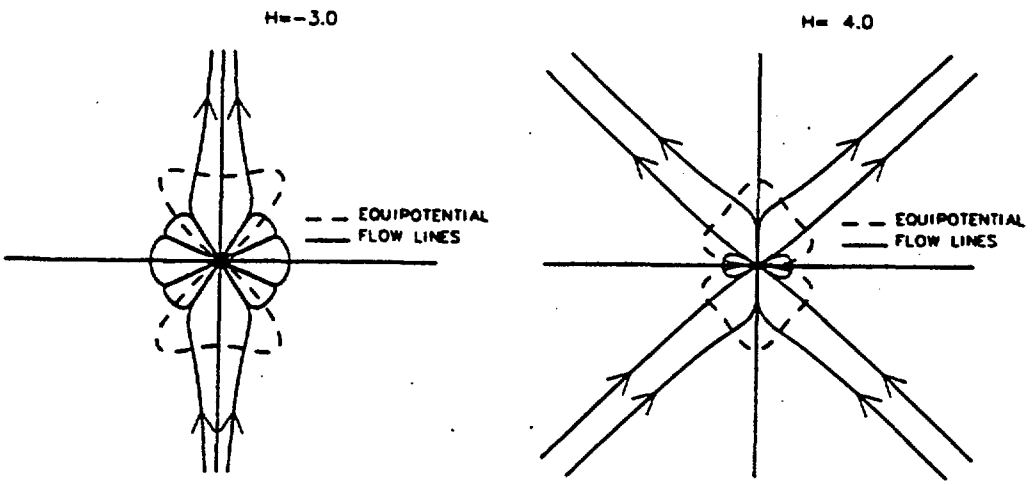

Fig. 7. Same as Figs. 5d and 6d, but plotted to a much larger scale, for H values (a) -3, and (b) 4. In the upper half-plane defects are repelled along the open flow lines towards a common plane. For H=-3 this plane is the $(1\bar{1}0)$ plane. For H = 4 there are two such planes, (010) and (100).

for H values outside the interval $-1 \leq H < H_0$, could be the basis for a second dislocation-controlled nucleation mechanism.

C. Defect Flow: Next consider the kinetics of defect migration to the (001) edge dislocation. The defect concentration, c, must satisfy the equation of continuity, eq. (8), which, when thermal diffusion is neglected, becomes

$$\frac{1}{D_f}\frac{\partial c}{\partial t} = \frac{\nabla\cdot(c\nabla U)}{kT} \quad . \tag{32}$$

When the dislocation-defect interaction energy U for the (001) edge dislocation, eq. (14), is introduced into eq. (32), one obtains

$$\lambda(\rho,\phi,\alpha)\frac{\partial c}{\partial \rho} + \mu(\rho,\phi,\alpha)\frac{\partial c}{\partial \phi} + \tau\frac{\partial c}{\partial t} = \nu(\rho,\phi,\alpha)\cdot c \tag{33}$$

where

$$\left.\begin{aligned} \lambda(\rho,\phi,\alpha) &= \frac{\sin\phi}{\rho^2}\cdot\frac{(1+\alpha x)}{(1-\alpha x^2)} \\ \mu(\rho,\phi,\alpha) &= -\frac{\cos\phi}{\rho^3}\cdot\frac{f(x,\alpha)}{(1-\alpha x^2)^2} \\ \nu(\rho,\phi,\alpha) &= 4\alpha\frac{\sin\phi}{\rho^3}\cdot\frac{g(x,\alpha)}{(1-\alpha x^2)^3} \quad , \end{aligned}\right\} \tag{34}$$

$$g(x,\alpha) \equiv 1-2x(2-3\alpha)-6x^2(1-\alpha)-\alpha x^3(2+x)(2-\alpha) \quad , \tag{35}$$

and τ is a temperature-dependent time parameter given by

$$\tau = \frac{kTb^2}{4D_f \varepsilon r_o^3 BK} . \tag{36}$$

The quantities ρ, α, x, $f(x,\alpha)$ are defined in eqs. (15), (17), (19) and (20), respectively.*

Drift Flow Solution: The solution of eq. (33) is obtained, in a straightforward manner, using the standard techniques for solving first-order partial differential equations. See, for example, Hildebrand (1962). The curves represented by the solutions of the subsidiary equations

$$\frac{d\rho}{\lambda(\rho,\phi,\alpha)} = \frac{d\phi}{\mu(\rho,\phi,\alpha)} = \frac{dt}{\tau} = \frac{dc}{\nu(\rho,\phi,\alpha)\cdot c} \tag{37}$$

are called characteristic curves of the partial differential equation (33). If these are denoted by $u_i(\rho,\phi,t) = k_i$ (constant), $i = 1,2,3$, then $F(u_1,u_2,u_3) = 0$, where F is an arbitrary function, represents the general solution of eq. (33). A particular solution is obtained by applying appropriate initial and boundary conditions to this general solution. The characteristic functions u_1,u_2,u_3 associated with eq. (37) are ρ/γ_1, ce^{γ_2}, and $(\rho^3\gamma_3/\gamma_1 - t/\tau)$. γ_1, γ_2, γ_3 are functions of the angle ϕ and the parameter α defined in eq. (17):

$$\gamma_1(\phi,\alpha) = \exp\left\{\int \frac{(1-\alpha x^2)(1+\alpha x)}{2(x+1)f(x,\alpha)}\, dx\right\} \tag{38}$$

*The ensuing discussion is given for $\varepsilon > 0$ so that the time parameter τ is positive. If $\varepsilon < 0$, a positive time parameter τ can still be defined by (36) with ε replaced by $|\varepsilon|$, necessitating the introduction of a minus sign before the third term in equation (33). The resultant depletion zone for a negative ε value will be rotated by 180° from that for the corresponding positive ε value (as noted previously, changing the sign of ε reverses the direction of defect motion along flow lines).

$$\gamma_2(\phi,\alpha) = 2\alpha \int \frac{g(x,\alpha)}{(x+1)(1-\alpha x^2)f(x,\alpha)}\, dx \tag{39}$$

$$\gamma_3(\phi,\alpha) = -\int \frac{(\gamma_1(\phi,\alpha))^3\,(1-\alpha x^2)^2}{\cos\phi \cdot f(x,\alpha)}\, d\phi\ . \tag{40}$$

A comparison of eq. (38) with eq. (18) shows that the curves given by $\rho = k_1\gamma_1(\phi,\alpha)$ are the flow lines along which the defects move to the dislocation. These curves, previously obtained as the orthogonal trajectories of the interaction potential (14), also represent a family of characteristics of the differential equation (33). The second set of characteristics gives the angular distribution of the defect concentration. The third set, the time-dependent characteristics, gives the depletion zone boundaries.

In the specific problem being considered, the initial concentration of defects is taken to be uniform, i.e. $c = c_o$ (constant) at $t = 0$, except at the dislocation center ($\rho = 0$) where $c = 0$ at all times. This last condition represents the sink for defects described in Section IIC. The solution of eq. (33) is then

$$c = 0 \tag{41}$$

within the closed region defined by the curve

$$\rho = \left(\frac{t}{\tau}\right)^{1/3} \frac{\gamma_1(\phi,\alpha)}{(\gamma_3(\phi,\alpha))^{1/3}} \equiv \left(\frac{t}{\tau}\right)^{1/3} \sigma(\phi,\alpha)\ . \tag{42}$$

This equation describes the time dependent depletion zone boundary. Outside the region defined by eq. (42) the concentration is given by

$$c = c_0 e^{\gamma_2(\phi,\alpha)} \quad . \tag{43}$$

The defect concentration is discontinuous across the expanding depletion zone boundary, eq. (42).

The function γ_1 was determined in obtaining the flow line solution and is given by the right-hand side of eq. (22). There are five different analytic forms for γ_1, depending on the value of H.

The functions γ_2 and γ_3 also depend on the anisotropy parameter H. Hence both the form of the depletion zone boundary equation and the equation for the concentration of defects outside the depletion zone will depend on the value of H.

Defect Distribution: The angular distribution function γ_2, defined by eq. (39), can always be evaluated analytically. There are five different analytic forms, depending on the value of H, corresponding to the forms encountered in the evaluation of γ_1. It should be pointed out that the expressions derived for γ_2 contain parameters which are rather complicated functions of x_1, x_2, x_3. However, it was found that by using the relations obtained from the coefficients of $f(x,\alpha) = 0$, namely

$$\begin{aligned} -\alpha(x_1+x_2+x_3) &= 3-2\alpha \\ \alpha(x_1x_2+x_2x_3+x_1x_3) &= -1 \\ -\alpha^2 x_1x_2x_3 &= 1-2\alpha \end{aligned} \tag{44}$$

the function γ_2 could be rewritten in terms of the same parameters contained in the function γ_1: specifically, e^{γ_2} is equal to

$$C_2|x+1|^{\frac{-H}{2(H+1)}}(1-\alpha x^2)^2\ |x-x_1|^{p_1-1}|x-x_2|^{p_2-1}|x-x_3|^{p_3-1} \qquad \begin{pmatrix}-4<H<-1\\ -1<H<0\\ H_o<H<\infty\end{pmatrix} \quad (45a)$$

$$C_2|x+1|^{\frac{-H}{2(H+1)}}(1-\alpha x^2)^2\ |x-x_1|^{p_1-1}\left((x-k)^2+\ell^2\right)^{q-1}\exp\left\{r\tan^{-1}\left(\frac{x-k}{\ell}\right)\right\} \qquad 0<H<H_o \quad (45b)$$

$$C_2|x+1|^{\frac{-H_o}{2(H_o+1)}}(1-\alpha_o x^2)^2\ |x-x_1|^{p_1-1}\ |x-x_o|^{\lambda_o-2}\exp\{\mu/(x_o-x) \qquad H=H_o \quad (45c)$$

$$C_2|x+1|^{-11/7}\ (3+x^2)^2|x-x_1|^{p_1-1}\ |x-x_2|^{p_2-2}\exp\left\{-\frac{2}{7(x+1)}\right\} \qquad H=-1 \quad (45d)$$

$$C_2 \qquad H=0 \quad (45e)$$

C_2 is a constant and the parameters p_1, p_2, p_3, q, r, λ_o, μ_o are the same as those defined previously in the corresponding expressions for γ_1, equations 23 to 28. In Eq. (45c), $\alpha_o = H_o/(4+H_o) \simeq 0.4727$.

The nature of the distribution function $e^{\gamma 2}$ can be ascertained by considering the various factors in eq. (45). The $|x-x_1|$ and $|1-\alpha x^2|$ terms are always positive. The $|x+1|$, $|x-x_2|$ and $|x-x_3|$ terms will be equal to zero at certain angles. The first term is zero at $\phi = \pm\pi/2$. The other two are zero, for particular ranges of H values, at angles ϕ_2, ϕ_3 defined in eq. (29) and shown in Fig. 4. Whether any of the $|x+1|$, $|x-x_2|$, $|x-x_3|$ terms represents a zero or infinity in the angular distribution function, $e^{\gamma 2}$, depends on the sign of the corresponding exponent in eq. (45). These statements are analogous to those given previously in the discussion on flow lines. However, note that the exponents in $e^{\gamma 2}$ are related to,

but different from, those in γ_1. Using eq. (45) and the results presented in Fig. 3 leads to the following conclusions: For $-1 \leq H < 0$ the angular distribution function consists of two symmetric closed curves, one on either side of the dislocation. For all values of H outside the interval $-1 \leq H \leq 0$ the function e^{γ_2} is unbounded at $\phi = \pm\pi/2$, even in the range $0 < H < H_0$ where the flow lines are closed. There are additional singularities at the four angles given by $x = x_2$ for $-4 < H \leq -2$ and $3.7 \lesssim H < \infty$, and also at the four angles given by $x = x_3$ for $-4 < H \lesssim -1.4$ and $H_0 \leq H < \infty$.

To illustrate some of these conclusions the defect concentration function, $c_0 e^{\gamma_2}$, (in arbitrary units) is plotted in Fig. 8 for H = -0.75, 0, 2, and 5. In an isotropic material (H = 0) the concentration of defects is uniform and polar plots of $c_0 e^{\gamma_2}$ are circular. In the range $-1 \leq H < 0$ the function e^{γ_2} contains pronounced peaks at certain angles. For example, in the plot for H = -0.75, which applies to unirradiated NaCl at ≈100C, the relative defect concentrations at angles of 0°, 40°, 73°, and 90° from the slip plane of the dislocation are 0.93, 0.43, 1, and 0, respectively. In the range $0 < H < H_0$ similar peaking occurs in addition to the singularities at $\phi = \pm\pi/2$, as illustrated in the plot for H = 2, Fig. 8c. Finally, the plot for H = 5 contains additional unbounded peaks at the angles given by $x = x_2, x_3$.

The singularities in the plots of defect concentration are a mathematical fiction introduced by the drift flow approximation. When applied to real crystals, these singularities indicate that the defect concentration will be high along certain planes. The actual concentration will be as high as possible consistent with other physical limitations. It is

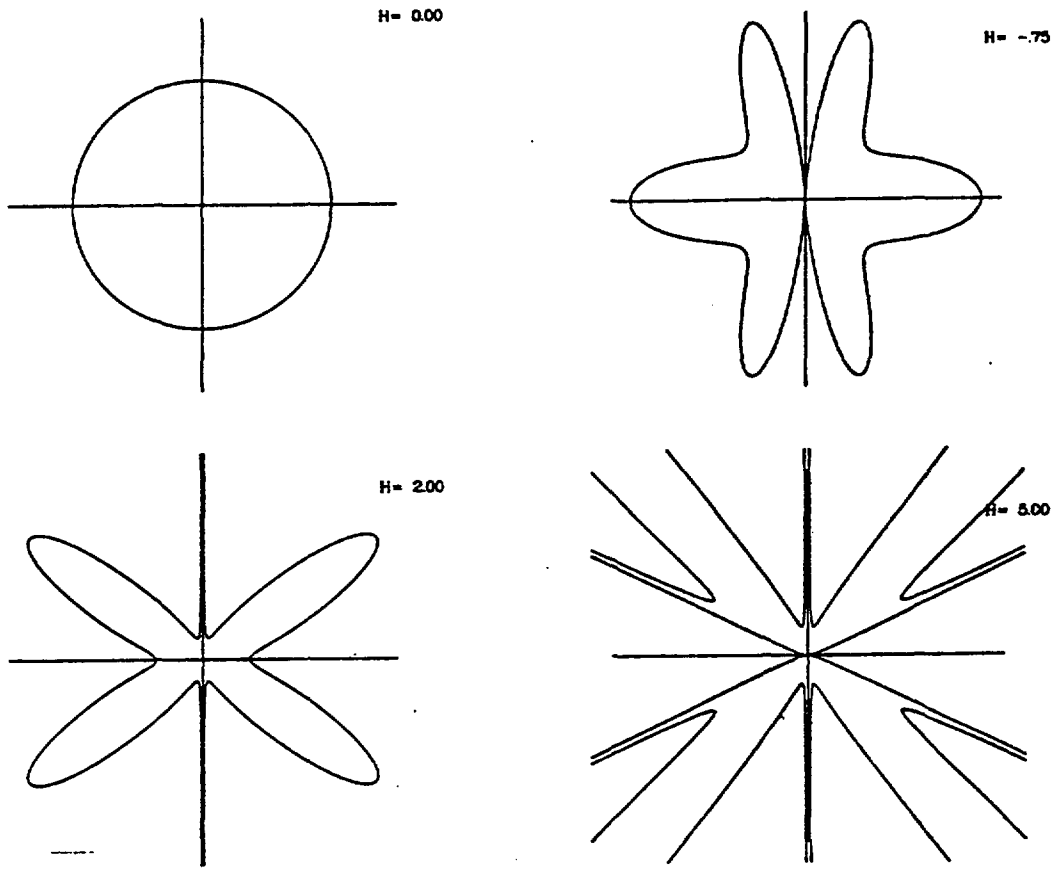

Fig. 8. The defect distribution function $c_o e^{\gamma_2}$, plotted in arbitrary units, for H values, equal to (a) 0, (b) −0.75, (c) 2 and (d) 5.

anticipated that the anisotropy-induced peaking in the defect concentration at certain angles will also be important in a calculation of defect migration when both drift flow and thermal diffusion are considered.

The last item about the function γ_2 to be discussed is the determination of the constant factor C_2 in eq. (45). First, note that the differential equation (33) is homogeneous only for an isotropic medium. The function $\nu(\rho,\phi,\alpha)$ defined in (34) is zero only if H = 0. Hence, for any non-zero value of H, the uniform defect concentration initial condition is not possible. In the drift flow solution the defects (outside the depletion zone) are distributed anisotropically according to eq. (45) at all times. Taking c_0 to be the average concentration at t = 0 and writing e^{γ_2} in the form

$$e^{\gamma_2} = C_2 e^{\lambda(\phi)} , \tag{46}$$

then C_2 is given as

$$C_2 = \left(\frac{1}{2\pi}\int_0^{2\pi} e^{\lambda(\phi)}d\phi\right)^{-1} = \left(\frac{1}{\pi}\int_{-\pi/2}^{\pi/2} e^{\lambda(\phi)}\,d\phi\right)^{-1} \tag{47}$$

The second expression in (47) follows from symmetry about the dislocation.

Depletion Zone: The function γ_3, defined by eq. (40), is required for the evaluation of the depletion zone boundary, eq. (42). It was not possible to evaluate analytically the integral in eq. (40). Hence γ_3 and the depletion zone boundaries were determined numerically for various values of H.

Before proceeding, it should be reemphasized that the principal reason for obtaining the depletion zone boundary is to calculate the number of defects that reach the dislocation per unit time, i.e. to compute the

defect flow as defined in eq. (9). In the range $-1 \leq H < H_0$ where the flow lines are closed the numerical determination of γ_3, and hence the depletion zone boundary, is straightforward. Outside the interval $-1 \leq H < H_o$ some of the flow lines are open, i.e. γ_1 has singularities. Since the integrand in the expression for γ_3 contains γ_1^3, the numerical determination of γ_3 is quite complicated. The function γ_3 will have singularities corresponding to those in γ_1, and it is only the depletion zone boundary, which depends on the ratio $\gamma_1/\gamma_3^{1/3}$, which is expected to remain finite at all angles. In addition, the expression for the defect flow will also involve the angular distribution function e^{γ_2} which, as shown in the previous section, has singularities for all H values outside the interval $-1 \leq H \leq 0$. Hence, even if an analytical expression for the zone boundary were known, the mathematical singularities in e^{γ_2} would greatly complicate numerical computations of the defect flow. This is particularly true for those singularities which occur for H values outside the interval $-1 \leq H < H_0$, such as shown for H = 5 in Fig. 8. From these two considerations it was decided (to save time and computing cost) to restrict the initial computations to values of H in the interval $-1 \leq H < H_0$.

Obviously the depletion zone will be symmetric about the dislocation. For all values of H in the interval $-1 \leq H < H_0$ the flow lines are closed. The defects enter the center of the dislocation at the angle $\phi = -\pi/2$, as is illustrated in Figs. 5, 6 for the cases H = -1, 0, 1, 3. Since this is true at all times, it is clear that $\rho(-\pi/2) = 0$, where ρ refers to the depletion zone boundary defined in eq. (42). Also, by a limiting process, one can show that $\rho(\pi/2) = (3t/\tau)^{1/3}$. Typical results

of computations are shown in Fig. 9 in which depletion zone boundaries are shown for H = -0.85, 0, 3.50, at the same t/τ value.

A number of interesting characteristics of depletion zone boundaries, for H values not in the range $-1 \leq H < H_0$, can be ascertained without making computations. These characteristics are associated with the open flow lines occurring for H values outside the interval $-1 \leq H < H_0$, as shown in Figs. 5, 6. The open flow lines below the slip plane continually bring defects to the dislocation. Hence depletion does not occur at the angles for which these flow lines exist. For example, for H values in the interval $H_0 \leq H < \infty$, the depletion zone is defined only for the interval $-\phi_2 < \phi < \pi+\phi_2$, where ϕ_2 is the acute angle defined in eq. (29) and shown in Fig. 4. In the limit as $H \to \infty$, $\phi_2 \to 0$ and the depletion zone is confined to the upper half-plane. The tendency for the region of excluded angles to develop as H increases from zero can be seen by comparing the H = 0 and H = 3.50 depletion zones in Fig. 9. The depletion zone boundary for H = 3.50 is defined for all angles ϕ but is hardly discernible in the figure in the vicinity of $\phi = -\pi/2$.

A similar result is obtained for H values in the range $-2 < H < -1$. In this case the depletion zone exists only for $-\phi_3 < \phi < \pi+\phi_3$ where the acute angle ϕ_3 is also defined in eq. (29) and shown in Fig. 4.

Likewise, for H values in the range $-4 < H < -2$ the depletion zone is defined only for $-\phi_3 < \phi < \pi+\phi_3$. In addition to the zeros in the depletion zone boundary at $\phi = -\phi_3, \pi+\phi_3$, zeros are also expected at the angles $\phi = \phi_2, \pi-\phi_2$ in the upper half-plane. These additional zeros are associated with the extra loops in the flow lines as illustrated in Fig. 6d. In other words, for $-4 < H < -2$, the depletion zone contains three

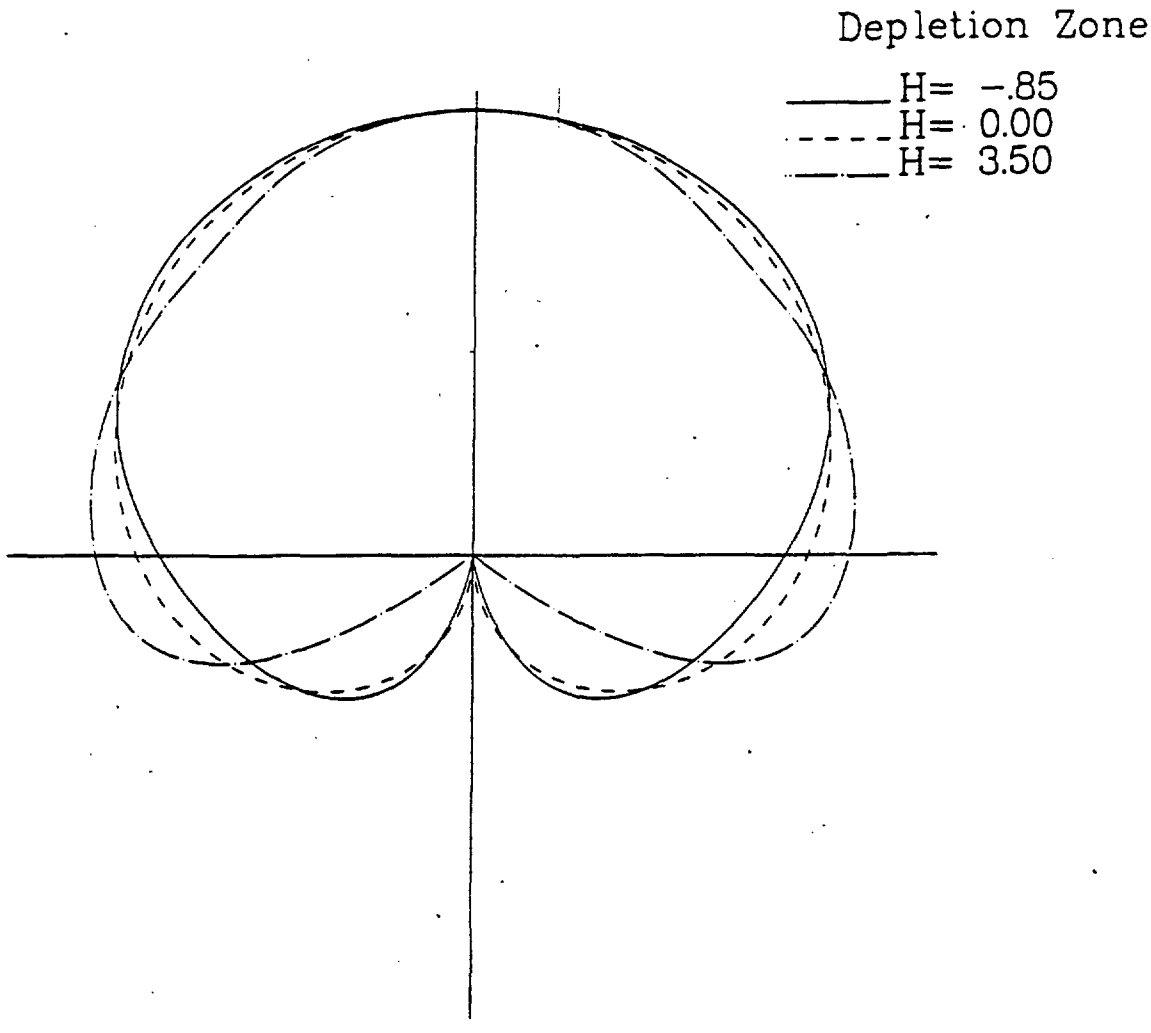

Fig. 9. The area, or depletion zone, normal to a <001> edge dislocation from which defects have been removed, by migrating to the dislocation, by the interaction between the strain field of the dislocation and the defect. These curves show the boundaries for various values of the anisotropy parameter H. The value H = -0.85 corresponds to unirradiated NaCl at room temperature. The axes lie along <110> directions.

lobes: one from $-\phi_3$ to ϕ_2, the second from ϕ_2 to $\pi-\phi_2$, and the third from $\pi-\phi_2$ to $\pi+\phi_3$. In the limit $H \to -4$, each lobe is 90° wide. Hence, for H values outside the interval $-1 \leq H < H_0$, anisotropy affects not only the shape but the nature of the depletion zone.

Temperature-dependent Time Parameter τ: The depletion zone boundary, defined by eq. (42), is a function of the reduced time (t/τ). The parameter τ, defined by eq. (36), depends on both the strength of the dislocation-defect interaction, E, and the defect diffusion coefficient, $D_f = D_0 \exp(-E_f/kT)$. Since the latter obviously varies exponentially with 1/T, in general τ will be a decreasing function of temperature. This is illustrated in Fig. 10 for NaCl, in which the time constant τ is plotted over the temperature range 24C-700C for two values of the misfit parameter ε. (As discussed in Section IIA, the misfit parameter ε is a measure of the volume change associated with the defect.) The τ values were calculated from eq. (36), using the elastic constant values reported by Hart (1968) and the diffusion coefficient for F-centers given by Jain and Lidiard (1977)

$$D_f = 0.01 \exp\{-0.8 \text{ eV}/kT\} \text{ cm}^2/\text{sec.} \qquad (48)$$

Since τ decreases with increasing temperature, the time required for the depletion zone to expand to a given dimension and, therefore, for a specific number of defects to reach the dislocation will likewise decrease with increasing temperature. A computation of the movement of F-centers to the <001> edge dislocation in NaCl, as indicated by the outward movement of the depletion zone, is illustrated in Figs. 11, 12 for crystals at 24C and 150C. Using the diffusion coefficient given by eq. (48) and a mis-

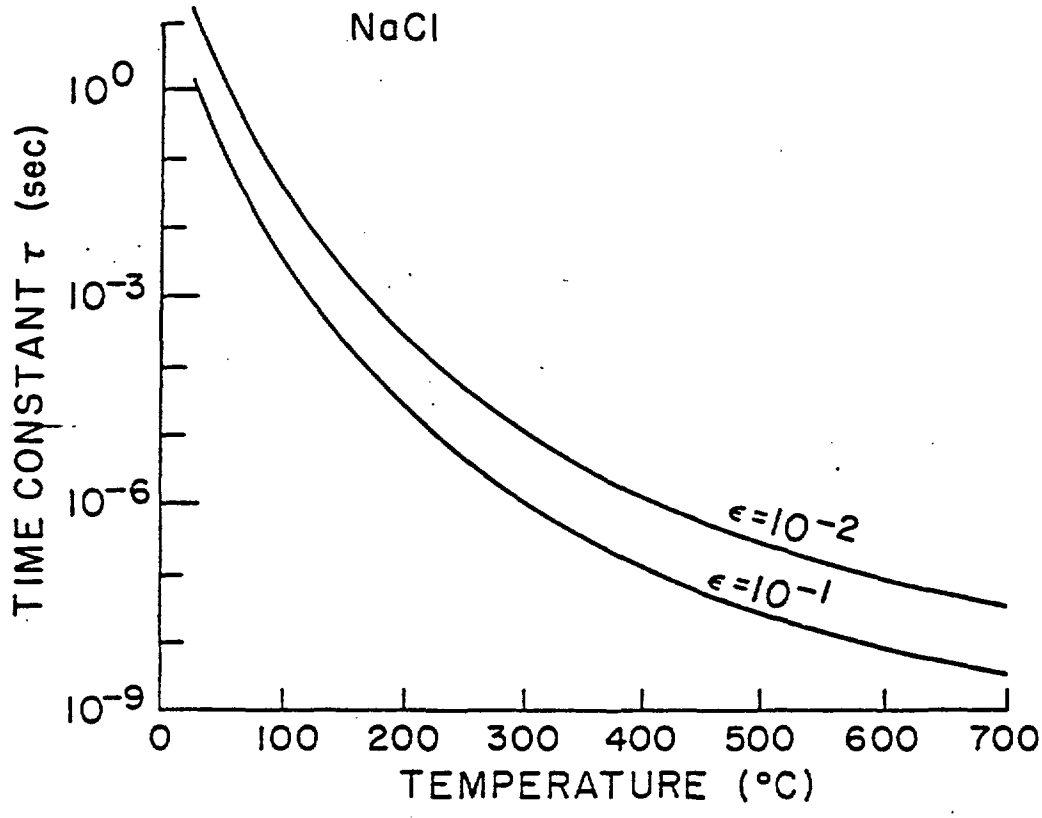

Fig. 10. The time constant τ associated with the migration of F-centers to a <001> edge dislocation in NaCl plotted as a function of temperature for two values of the misfit parameter ε.

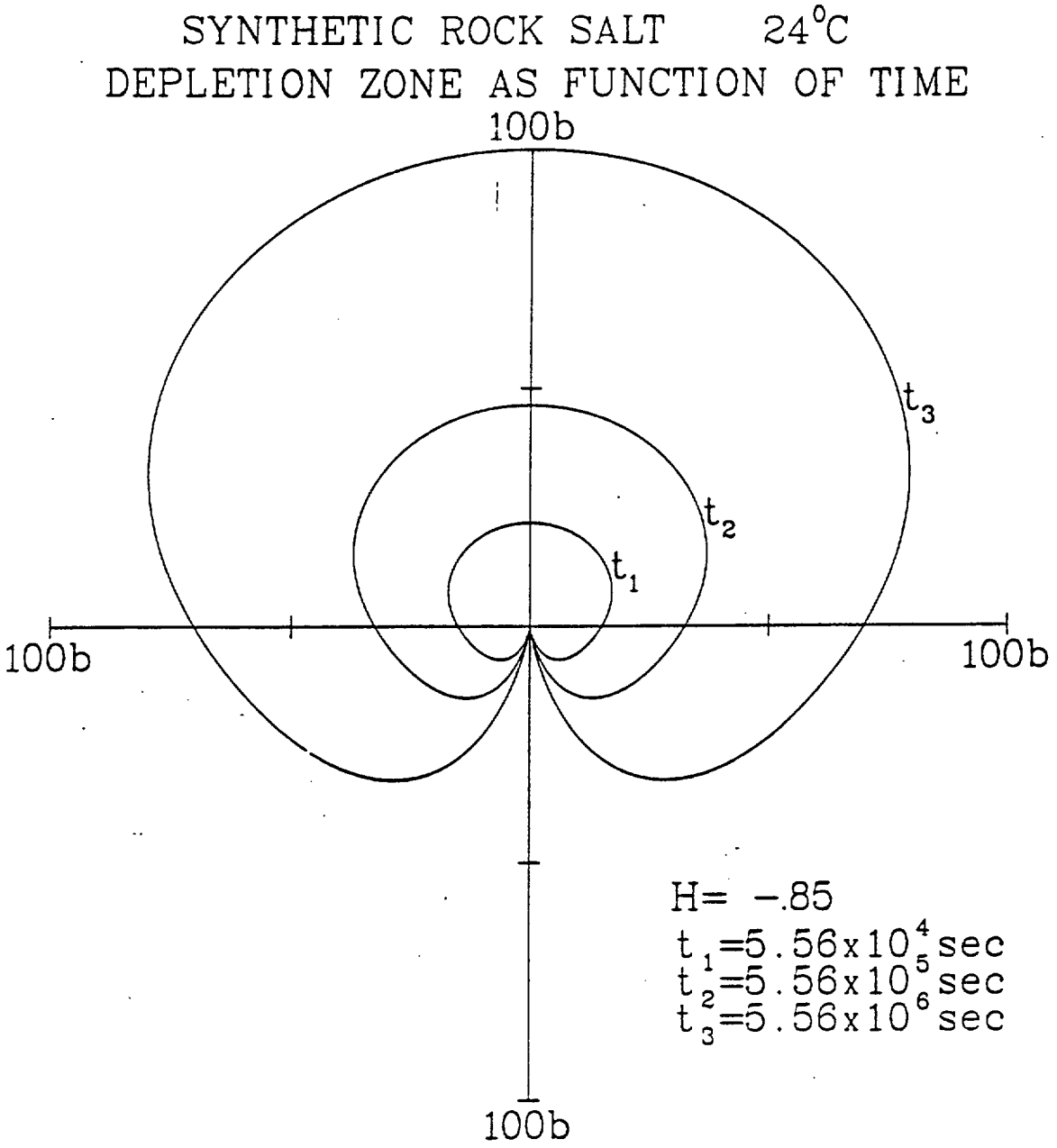

Fig. 11. Depletion zone boundaries, normal to a <001> edge dislocation in NaCl at room temperature, as a function of time after defects have been introduced into the lattice. The axes lie along <110> directions. The units are Burgers vectors; 100 b = $\sqrt{2}/2$ x 100 lattice constants.

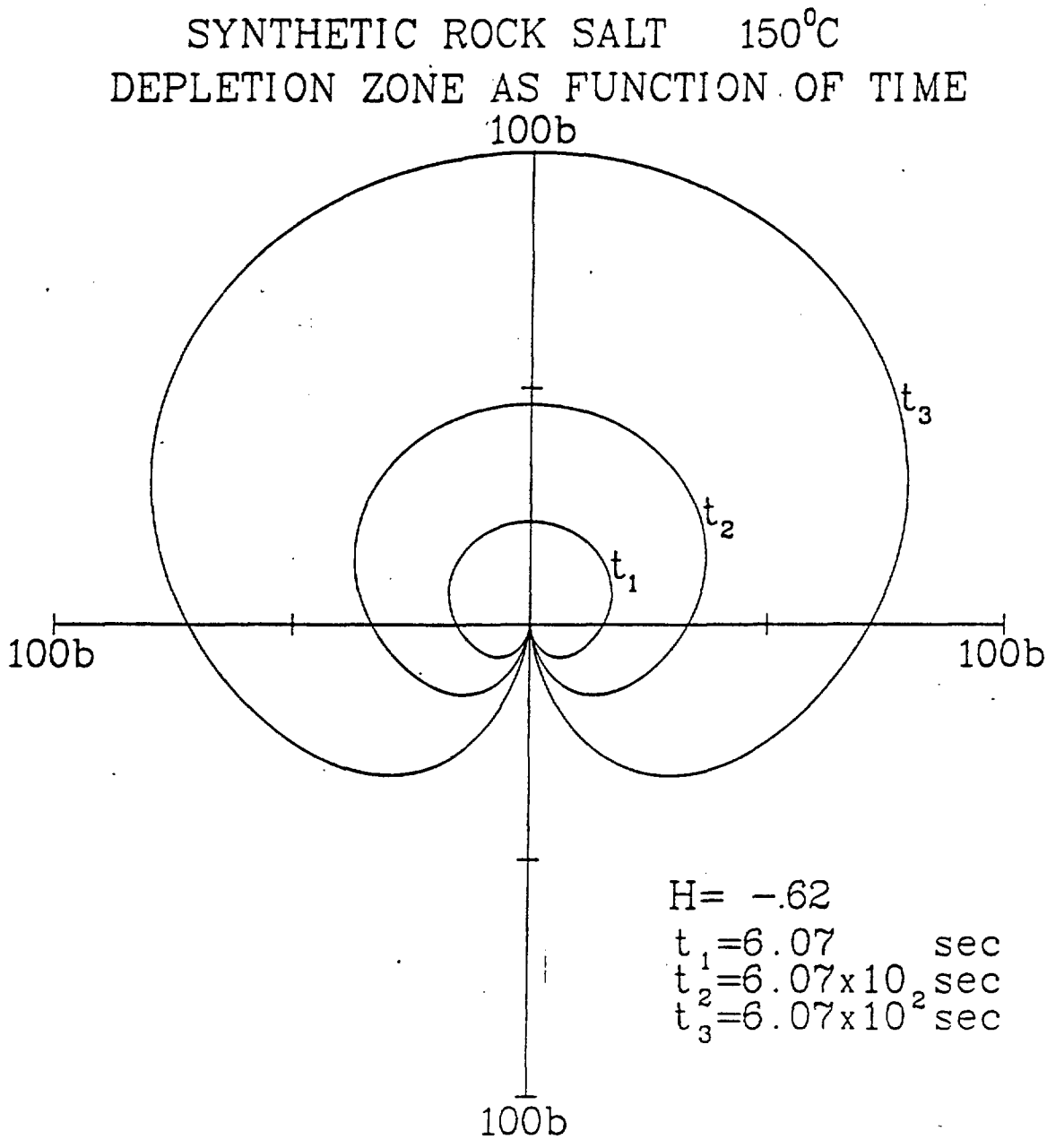

Fig. 12. Same as Fig. 11 except that the crystal is at 150C instead of 24C.

fit parameter $\epsilon = 0.02$, the τ values at 24C and 150C are 16.88 seconds and 1.820×10^{-3} seconds, respectively. The H values at these temperatures are -0.85 and -0.62. At both temperatures the depletion zone boundaries are shown for three times t_1, t_2, t_3. Although these times correspond to the same multiples of $(\tau/3)$ at the two temperatures (namely, 10^4, 10^5, and 10^6), the physical times at the two temperatures are quite different. At 150C, the three times are t_1, t_2, t_3 = 6.07 sec, 60.7 sec, and 607 sec, respectively. At 24C the three times are t_1, t_2, $t_3 = 5.56 \times 10^4$ sec, 5.56×10^5 sec, and 5.56×10^6 sec, respectively. Obviously, the depletion process is strongly temperature dependent. For the depletion zone to reach a dimension of 100 Burgers vectors ($\sqrt{71}$ lattice constants) at room temperature requires more than two months. At 150C the corresponding time is approximately ten minutes. It is interesting to note that these calculated times are in line with experimental observations. When a sample is irradiated at room temperature and then stored in the dark, colloids are observed to form in two to six months. In contrast, samples irradiated at 150C usually form colloids during irradiation. The temperature dependence of the depletion process will be discussed in greater detail in the section below on depletion times.

Number of Defects Reaching the Dislocation: Once the depletion zone is known, the defect flow, N(t), can be calculated from eq. (9). N(t), the number of defects which arrive at the dislocation as a function of time, is given by an integration of the defect density over the area of the depletion zone:

$$N(t) = \frac{c_0 b^2}{2} \int_0^{2\pi} e^{\gamma_2 \rho^2} d\phi = c_0 b^2 \int_{\pi/2}^{\pi/2} e^{\gamma_2 \rho^2} d\phi \qquad (49)$$

where ρ represents the depletion zone boundary, and the second expression follows from symmetry about the dislocation. With the aid of eqs. (42), (46), and (47) this last expression for N(t), eq. (49), can be rewritten as

$$N(t) = c_0 b^2 \left(\frac{t}{\tau}\right)^{2/3} \psi(H) \tag{50}$$

where

$$\psi(H) \equiv \frac{\int_{-\pi/2}^{\pi/2} e^{\lambda} \sigma^2 d\phi}{\frac{1}{\pi} \int_{-\pi/2}^{\pi/2} e^{\lambda} d\phi} \quad . \tag{51}$$

The defect flow is proportional to the two-thirds power of the reduced time. All dependence on the anisotropy parameter is contained in the function ψ (H).

Over the range of H values $-1 \leq H \leq 0$, both σ and e^{λ} are bounded, and the numerical evaluation of the two integrals in (51) is straightforward. For $0 < H < H_0$ there are singularities in e^{λ} at $\phi = \pm\pi/2$ in both integrals in eq. (51). To evaluate these integrals, write

$$e^{\lambda(\phi)} = |x+1|^{-Z} A(x,H) \tag{52}$$

where, from eq. (45b), $Z = H/2(H+1)$, and

$$A(x,H) = (1-\alpha x^2)^2 \, |x-x_1|^{P_1-1} \left((x-k)^2+\ell^2\right)^{q-1} \exp\left\{r \tan\left(\frac{x-k}{\ell}\right)\right\} \tag{53}$$

First consider the integral in the denominator of (51). To eliminate the singularity, write the integral

$$\frac{1}{C_2} = \frac{1}{\pi}\int_{-\pi/2}^{\pi/2} |x+1|^{-Z}\, A(x,H)\,d\phi \qquad (54)$$

as

$$\frac{1}{C_2} = \frac{2}{\pi}\int_{0}^{\pi/2} |x+1|^{-Z}\, A(-1,H)\,d\phi + \frac{2}{\pi}\int_{0}^{\pi/2} |x+1|^{-Z}\, \{A(x,H) - A(-1,H)\}\,d\phi. \qquad (55)$$

See, for example, Davis and Rabinowitz (1967). The integrand in the second integral is well behaved, and this integral can be computed numerically. The first integral can be integrated to give

$$\frac{A(-1,H)}{\frac{-H}{2^{2(H+1)}\sqrt{\pi}}}\;\frac{\Gamma\left(\frac{1}{2(H+1)}\right)}{\Gamma\left(\frac{(H+2)}{2(H+1)}\right)}$$

where Γ is the gamma function. Hence $1/C_2$ can be determined.

An analogous procedure is utilized to evaluate the integral over the depletion zone in the numerator of eq. (51) for H values in the range $0 < H < H_0$. One writes

$$\int_{-\pi/2}^{\pi/2} e^{\lambda\sigma^2}d\phi = \int_{-\pi/2}^{0} e^{\lambda\sigma^2}d\phi + \int_{0}^{\pi/2} 3^{2/3}\, A(-1,H)\, |x+1|^{-Z}\, d\phi \qquad (56)$$

$$+ \int_{0}^{\pi/2} |x+1|^{-Z}\, (\sigma^2 A(x,H) - 3^{2/3} A(-1,H))\,d\phi\ .$$

Since $\sigma(-\pi/2) = 0$ and $\sigma(\pi/2) = 3^{1/3}$, the integrands in the first and third integrals on the right-hand side of eq. (56) are well behaved, and, hence, these integrals can be evaluated numerically. The second integral is

integrable in terms of gamma functions, as in (55). Hence the numerator of $\psi(H)$ in eq. (51) can also be determined for $0 < H < H_0$.

It should be pointed out that the function $\psi(H)$ can be written solely in terms of the functions γ_1, γ_2, γ_3 obtained in the solution of the differential equation for the defect concentration, i.e.

$$\psi(H) = \int_{-\pi/2}^{\pi/2} \frac{e^{\gamma_2}\gamma_1^2}{\gamma_3^{2/3}}\, d\phi \ . \tag{57}$$

Using eq. (40) this can be converted to an integral over γ_3 which reads

$$\psi(H) = \int_{\gamma_3(\pi/2)}^{\gamma_3(-\pi/2)} Q(\phi,\alpha)\gamma_3^{-2/3}\, d\gamma_3 \tag{58}$$

where

$$Q(\phi,\alpha) \equiv \frac{\cos\phi \cdot f(x,\alpha)}{(1-\alpha x^2)^2}\ \frac{e^{\gamma_2}}{\gamma_1} \ . \tag{59}$$

Utilizing eqs. (22) and (45) one finds that, over the entire interval $-1 \leq H < H_0$, the function $Q(\phi,\alpha)$ reduces to a constant $Q_0(H)$ which depends on H value: specifically,

$$Q_0(H) = \begin{cases} \dfrac{C_2\alpha^2}{\sqrt{2}} & -1 < H < 0,\ 0 < H < H_0 \\ \dfrac{C_2}{\sqrt{2}} & H = 0,\ -1 \end{cases} \tag{60}$$

Hence, from eq. (58), one obtains that

$$\psi(H) = 3Q_0(H)\ \{\gamma_3(-\pi/2)\}^{1/3} \qquad -1 \leq H < H_0 \tag{61}$$

since $\gamma_3(\pi/2) = 0$ for these values of H. In other words, for values of H in the interval $-1 \leq H < H_0$, it is possible to obtain $\psi(H)$ by merely evaluating the integral γ_3 at one value of ϕ. The integration over the depletion zone is completely eliminated by this method. However, since the constant C_2 appears in $Q_0(H)$, the problem of dealing with any singularities in $e^{\lambda(\phi)}$ is not completely eliminated.

Hence, for H values in the interval $-1 \leq H < H_0$, it is possible to obtain $\psi(H)$, and hence the defect flow N(t), by two methods represented by eqs. (51) and (61). Computations of $\psi(H)$ were made by both methods for a series of H values in the interval $-1 \leq H < H_0$. Both methods gave identical results. It was found that, over the interval $-1 \leq H < H_0$, the function $\psi(H)$ passes through a maximum at $H = 0$: specifically, $\psi(-1) \simeq 3.378$, $\psi(0) = 3(\pi/2)^{1/3} \simeq 3.487$, and $\psi(3.5) \simeq 3.227$. All values of $\psi(H)$ in this interval of H are within 8% of the $\psi(0)$ value. In other words, over the range of H values $-1 \leq H < H_0$ (for which the flow lines are closed), the quantity $\psi(H)$, and therefore the defect flow N(t), is relatively insensitive to the value of the anisotropy parameter H.

The determination of $\psi(H)$ for values of H outside the interval $-1 \leq H < H_o$ poses similar but more complicated computational difficulties than those discussed above. Not only are there singularities in $e^{\lambda(\phi)}$ at $\phi = \pm\pi/2$, but (for almost all these H values) also at angles given by $x = x_2, x_3$, as discussed in the section on defect distribution. There are two methods to evaluate $\psi(H)$, represented by eqs. (51) and (58). Both methods must deal with the singularities in $e^{\lambda(\phi)}$, at least in the computation of C_2 which is common to both methods. The first method involves integration of the defect density over the depletion zone (numerator of the right-hand

side of eq. (51)) and again involves the singularities in $e^{\lambda(\phi)}$. For values of H outside the interval $-1 \leq H \leq H_0$ the depletion zone is not defined for all angles ϕ. This is connected with the presence of open flow lines for these values of H, as discussed in the section on depletion zones. The lower limit on the integral over the depletion zone in eq. (51) is not $\phi = -\pi/2$ but rather a function of H given by $\phi = -\phi_2$ for $H_0 < H < \infty$, and $\phi = -\phi_3$ for $-4 < H < -1$.

The second method for evaluating $\psi(H)$, eq. (58), is an integral along γ_3 which can be expressed in terms of γ_3 functions at various angles. It is to be recalled from eq. (40) that the function γ_3 is itself an integral whose integrand contains γ_1^3. For values of H outside the interval $-1 \leq H < H_0$ the function γ_1 contains singularities associated with the open flow lines. These singularities would have to be dealt with in the numerical evaluation of each γ_3 integral. Hence for H values outside the interval $-1 \leq H < H_0$ both methods for determining defect flow will involve computational difficulties.

Depletion Times: The depletion zone boundary expands with time. This has previously been illustrated in Figs. 11 and 12. The depletion time t_A is defined as the time required for the depletion zone to sweep out an area A. From eq. (42) t_A is found to be

$$t_A = \left(\frac{2A}{a^2\Sigma(H)}\right)^{3/2} \tau = \left(\frac{2A}{a^2\Sigma(H)}\right)^{3/2} \left(\frac{kTa^2 e^{E_f/kT}}{8\epsilon r_o{}^3 BKD_o}\right) \tag{62}$$

where a is the lattice parameter, τ is defined by eq. (36), and

$$\Sigma(H) \equiv \int_{-\pi 2}^{\pi/2} \left(\sigma(\phi,\alpha)\right)^2 d\phi \,. \tag{63}$$

The depletion times associated with the migration of F-centers to the <001> edge dislocation in rock salt have been computed for temperatures of 24, 100, 150, and 300C. The corresponding values of H in rock salt at these temperatures are -0.853, -0.697, -0.607, and -0.284, respectively. These H values were obtained from the elastic constant data for unirradiated NaCl (Hart, 1968). The same data were used to compute the values of B and K. D_0 was taken to be 0.01 cm^2/sec (Jain and Lidiard, 1977). The depletion times are plotted as a function of area in Figs. 13-16. For each of the four temperatures curves are shown for misfit parameter ϵ values 0.01 and 0.1, and for activation energy E_f values 0.4, 0.8, and 1.2 eV. These are believed to be suitable values for F-centers in NaCl.

Obviously, the larger the misfit parameter, i.e. the stronger the dislocation-defect interaction, the shorter will be the time required to sweep out a particular area at a given temperature. Increasing ϵ by a factor of ten (for the same value of E_f) decreases the depletion time by a factor of ten. Also, decreasing the value of the activation energy for diffusion E_f will decrease the time required to sweep out a given area at any temperature. For example, at 150C and for a misfit parameter ϵ = 0.01, decreasing the activation energy from 1.2 eV to 0.4 eV decreases the time required to sweep out an area of $10^4\ a^2$ from 4.36×10^7 sec (approximately 1.38 years) to 1.28×10^{-2} sec.

Next, consider the number of defects which have migrated to the dislocation at the depletion time t_A. Combining eqs. (50) and (62), one obtains

$$N(t_A) = c_0 A \frac{\psi(H)}{\Sigma(H)} . \qquad (64)$$

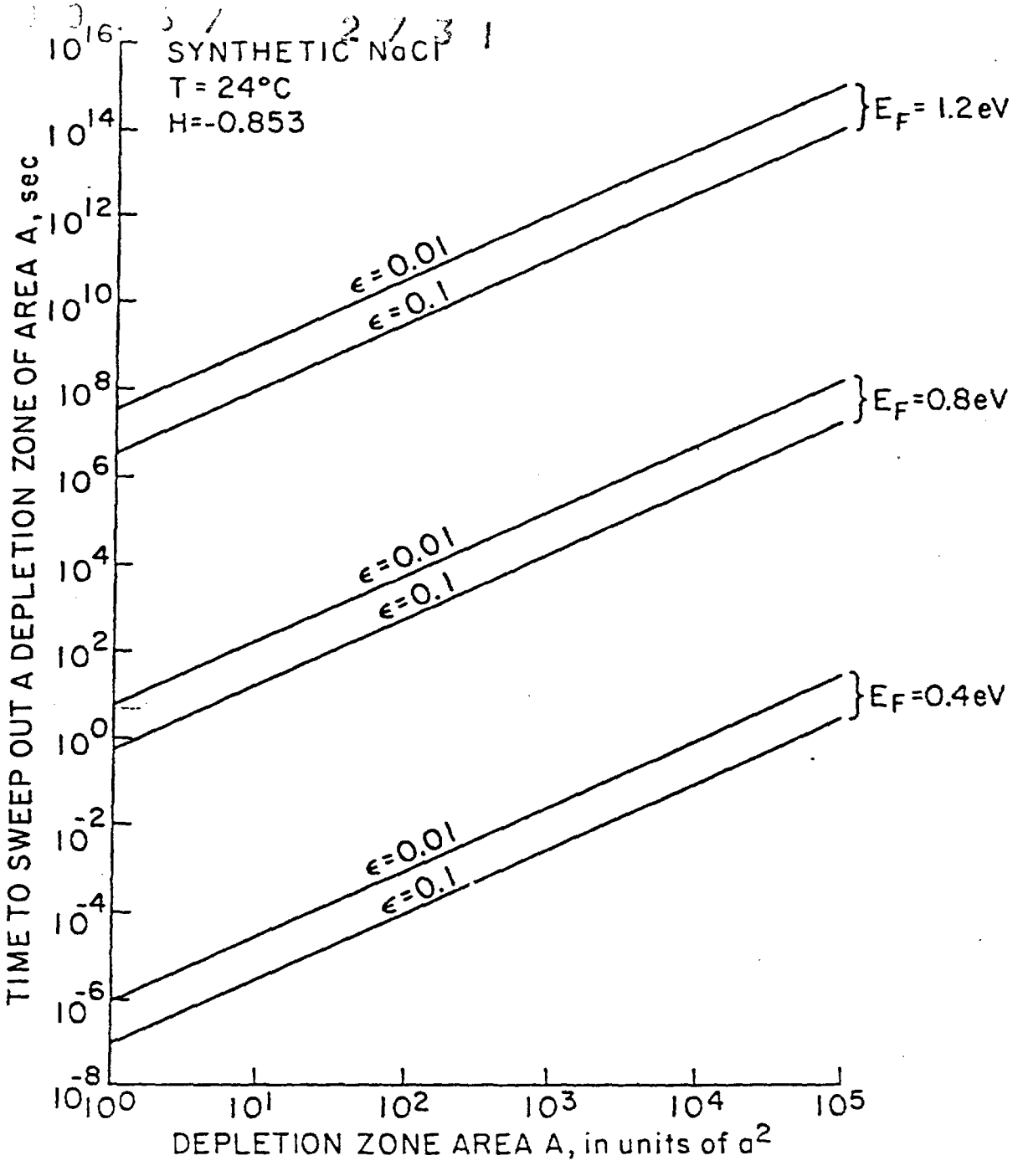

Fig. 13. The depletion times associated with the migration of F-centers at 24 °C to the <001> edge dislocation in rock salt plotted as a function of depletion zone area. Depletion times are shown for values of the misfit parameter ϵ equal to 0.01 and 0.1, and for values of the activation energy E_f equal to 0.4, 0.8, and 1.2 ev. These are believed to be suitable values for F-centers in NaCl.

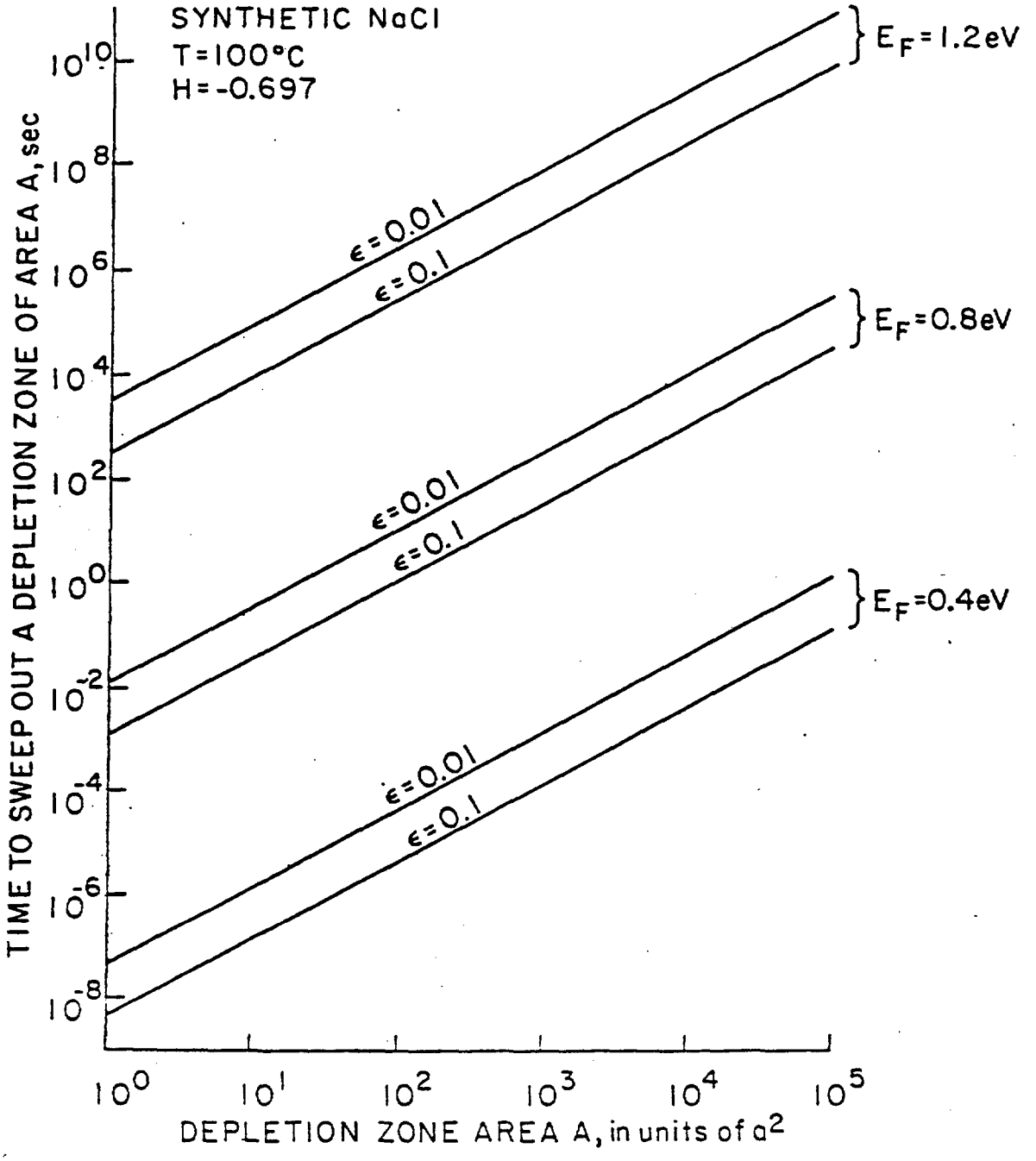

Fig. 14. Same as Fig. 13 except T = 100°C.

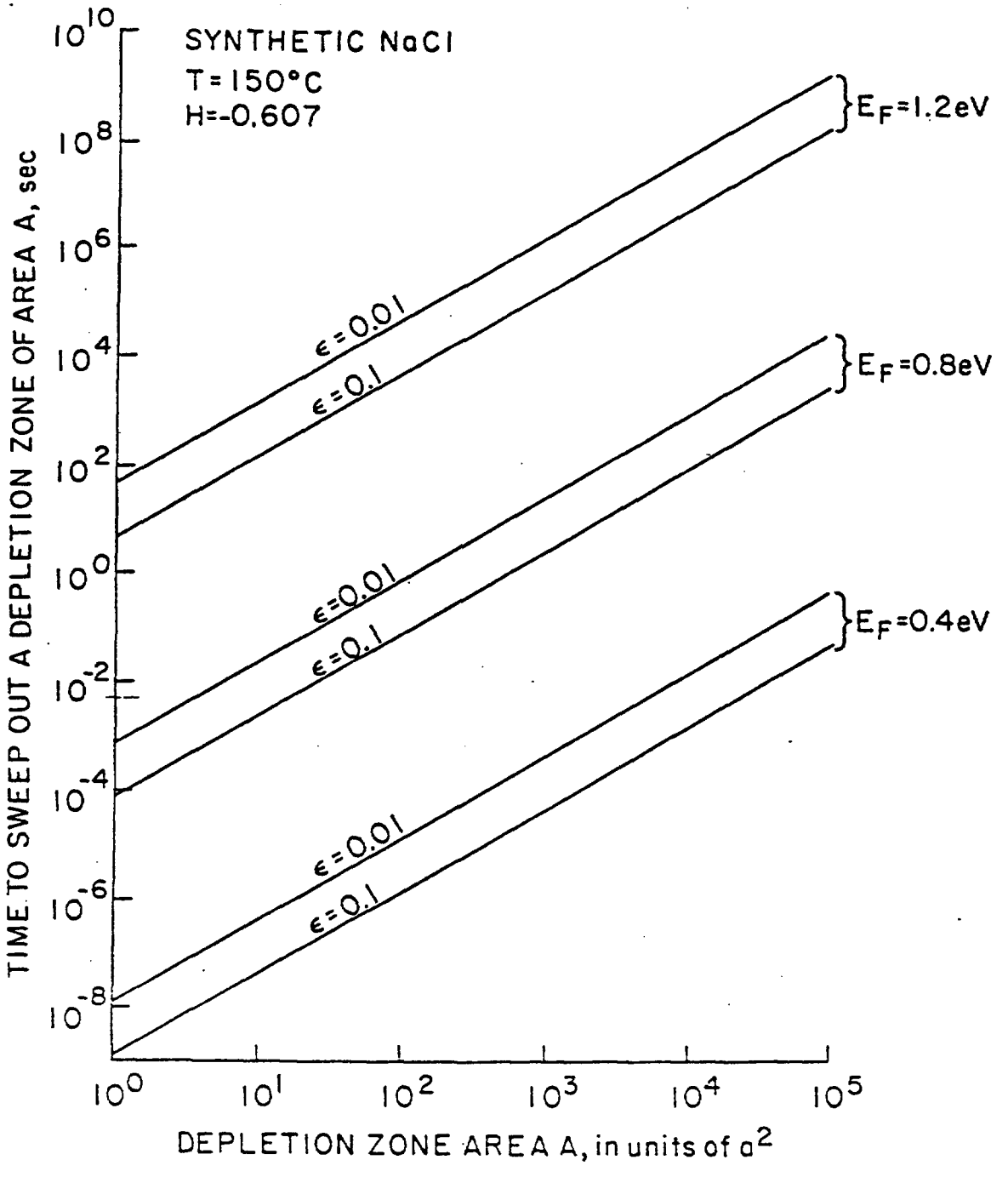

Fig. 15. Same as Fig. 13 except T = 150°C.

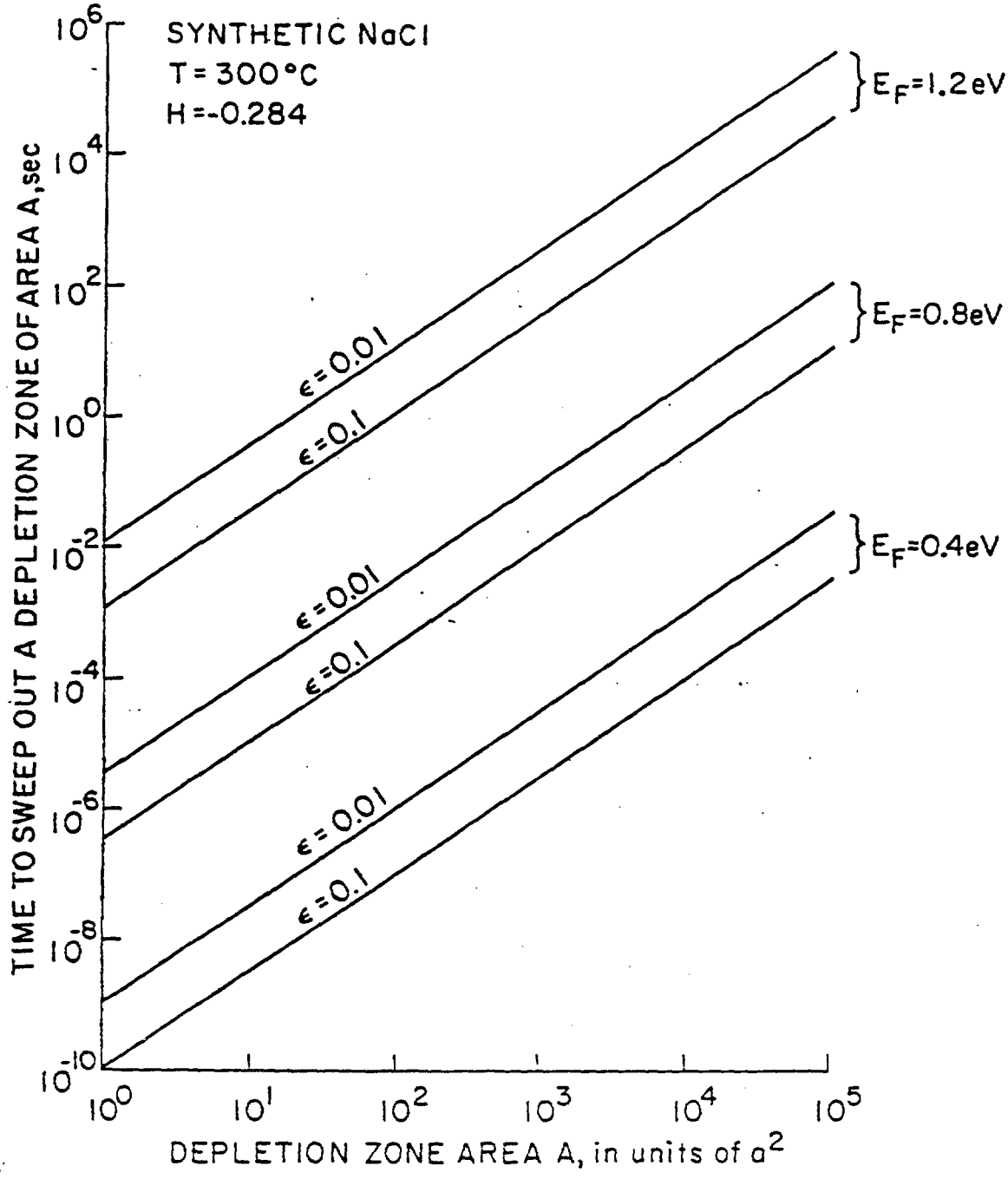

Fig. 16. Same as Fig. 13 except T = 300°C.

This is the number of defects per unit length which have arrived at the dislocation when a depletion zone of area A has been swept out. For a relatively long dislocation of length ℓ the total number of defects n for which the dislocation has acted as a sink (neglecting end effects) is

$$n = \ell \cdot N(t_A) = c_0 A \ell \frac{\psi(H)}{\Sigma(H)} \quad . \tag{65}$$

n is the number of defects removed from a cylinder about the dislocation line whose cross section normal to the dislocation is the depletion zone (42) at time t_A. One needs to estimate how large the depletion zone area must be in order that the number n be relevant to colloid nucleation in rock salt. For the values of H being dealt with here, $\psi(H)/\Sigma(H) \simeq 1$. Taking $c_0 = 10^{15}$ cm^{-3}, $\ell = 5 \times 10^{-4}$ cm, and $A = 10^s$ a^2, one obtains $n \simeq (1.6)10^{(s-3)}$. Hence the depletion zone area would have to be at least 10^3 a^2 for n to be physically significant, and probably 10^4 a^2 to be of relevance to colloid nucleation.

The time required to sweep out a depletion zone area of 10^4 a^2 about the <001> edge dislocation in rock salt is a function of temperature. This is illustrated in Fig. 17 in which the depletion times for an area of 10^4 a^2 are plotted over the temperature range of interest for colloid formation in rock salt, 24C-300C. Curves are shown for misfit parameters ε = 0.01, 0.1 and activation energies E_f = 0.4, 0.8, and 1.2 eV. The depletion process is strongly temperature dependent. For example, for a misfit parameter ε = 0.01 and an activation energy for diffusion E_f = 0.8 eV, the times required to sweep out a depletion zone of 10^4 a^2 at the four tempera-

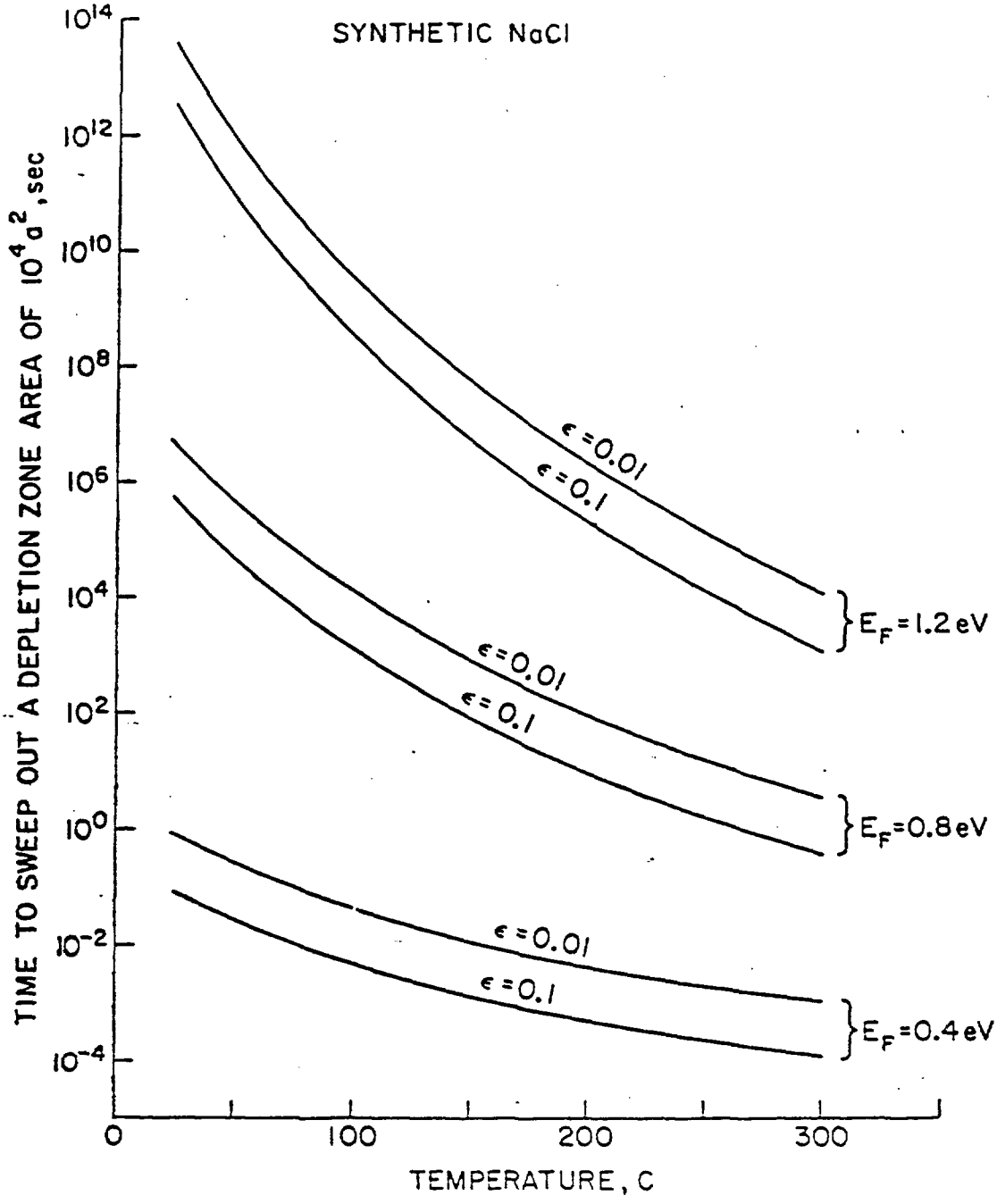

Fig. 17. The time required to sweep out a depletion zone area of $10^4 a^2$ about the <001> edge dislocation in rock salt plotted as a function of temperature. Curves are shown for various values of the misfit parameter ϵ and activation energy E_f which are considered suitable for F-centers in NaCl.

tures 24, 100, 150, and 300C are 5.61×10^6, 1.23×10^4, 7.46×10^2, and 3.54 sec, respectively.

Hence it is seen that for reasonable values of the parameters involved (defect density, dislocation length, misfit parameter, diffusion activation energy), sufficient defects will accumulate at the <001> edge dislocation in times that are consistent with experimental observations of colloid formation. The results thus indicate that the <001> edge dislocation is a viable site for colloid particle nucleation in rock salt.

ACKNOWLEDGMENT

The author would like to express his sincere thanks to Dr. P.W. Levy for his constant counsel, support and encouragement during the course of this study.

REFERENCES

F. Agullo-Lopez and P.W. Levy, 1964. Effects of gamma-ray irradiation on the mechanical properties of NaCl single crystals. Proc. Brit. Ceramic Soc. 1, 183.

R.L. Bradshaw and W.C. McLain, editors, 1971. Project Salt Vault: A Demonstration of the Disposal of High Activity Solidified Waste in Underground Salt Mines, Oak Ridge National Laboratory Report ORN L4555.

R. Bullough and R.C. Newman, 1970. The Kinetics of Migration of Point Defects to Dislocations, Rep. Prog. Phys. 33, 101.

R. Chang, 1962. The Dilatational Strain Field Associated with Edge Dislocations and Edge Dislocation Walls Based on Anisotropic Elasticity, Acta Met. 10, 951.

Y.T. Chou, 1963. Characteristics of Dislocation Stress Fields due to Elastic Anisotropy, J. Appl. Phys. 34, 429.

A.H. Cottrell, 1953. Dislocations and Plastic Flow in Crystals, Oxford University Press, London, p. 56.

J.H. Crawford, Jr. and L.M. Slifkin, editors, 1972. Point Defects in Solids, Vol. I, General and Ionic Crystals, Plenum Press, New York.

P.J. Davis and P. Rabinowitz, 1967. Numerical Intergration, Blaisdell Publishing Company, Waltham, Massachusetts, pp. 72-73.

G.E. Elgort and P.W. Levy, 1982. Thermally Induced Colloid Formation in Previously Irradiated Natural and Synthetic Rock Salt. (In preparation).

W.B. Fowler, editor, 1968. Physics of Color Centers, Academic Press, New York.

S. Hart, 1968. The Temperature Dependence of the Elastic Compliances of Some Alkali Halides," Brit. J. Appl. Phys. (J. Phys. D) 1, 1285.

S. Hart, 1977. The High-temperature Elastic Moduli of Alkali Halides, J. Phys. D: Appl. Phys. 10, L261.

F.B. Hildebrand, 1962. Advanced Calculus for Applications, Prentice-Hall, Inc., Englewood Clifs, New Jersey, Chapter 8.

L.W. Hobbs, 1973. Transmission Electron Microscopy of Defects in Alkali Halides. J. Physique Colloq. 34, C9-227.

L.W. Hobbs, A.E. Hughes and D. Pooley, 1973. A Study of interstitial Clusters in Irradiated Alkali Halides Using Direct Electron Microscopy, Proc. R. Soc. Lond. A, 167-185.

L.W. Hobbs, 1975. Transmission Electron Microscopy of Extended Defects in Alkali Halide Crystals, Surface and Defect Properties of Solids 4, Chem. Soc. Specialist Period Reports, London, p. 152.

U. Jain and A.B. Lidiard, 1977. The Growth of Colloidal Centres in Irradiated Alkali Halides, Phil. Mag. 35, 245.

R.W. Klaffky, K.J. Swyler, and P.W. Levy, 1979. Radiation Damage Studies on Synthetic NaCl Crystals and Natural Rock Salt for Waste Disposal Applications, II. Ceramics in Nuclear Waste Management, DOE Conference 790420 (Proc. of an Int. Sym.) T.D. Chikalla and J.E. Mendel, editors (U.S. Dept. of Energy, Washington) pp. 310-314.

R.W. Klaffky, K.J. Swyler, and P.W. Levy, 1982. Properties of Radiation Induced Colloid Particles in Synthetic NaCl Crystals and Natural Rock Salt. (In preparation).

P.W. Levy, K.J. Swyler, and R.W. Klaffky. Radiation Induced Color Center and Colloid Formation in Synthetic NaCl and Natural Rock Salt, Third

Europhysics Topical Conf., Lattice Defects in Ionic Crystals, J. de Physique 41, Supplement-Colloque C6, pp. 344-347 (1980).

P.W. Levy, 1981. Color Centers, Encyclopedia of Physics, R.G. Lerner and G.R. Trigg, editors (Addison-Wesley, Reading, MA), p. 131.

P.W. Levy, J.M. Loman, K.J. Swyler, and R.W. Klaffky, 1981. Radiation Damage Studies on Synthetic NaCl Crystals and Natural Rock Salt for Radioactive Waste Disposal Applications, to be published in: Advances in the Science and Technology of the Management of High Level Nuclear Waste, P.L. Hofmann, ed.

P.W. Levy, J.M. Loman, K.J. Swyler, and D.R. Dougherty, 1982. Recent Studies on Radiation Induced F-center and Colloid Particle Formation in Synthetic NaCl and Natural Rock Salt, Proc. 4th Europhysical Topical Conf. on Lattice Defects in Ionic Crystals, Dublin, Ireland. To be published in Radiation Effects.

P.W. Levy, 1983. Radiation Damage Studies on Natural Rock Salt from Various Geological Localities of Interest to the Radioactive Waste Disposal Program, Proc. Third Argonne Workshop on Basic Problems in Nuclear Waste, Argonne, IL, October 1981. To be publihsed in Nuclear Technology 60, No. 2, February 1983.

J.M. Loman, P.W. Levy, and K.J. Swyler, 1981. Radiation Induced Sodium Metal Colloid Formation in Natural Rock Salt from Different Geological Localities, to be published in Proc. 4th Materials Res. Soc. Symp. on the Scientific Basis of Nuclear Waste Mgmt., Boston, MA.

J.J. Markham, 1966. F-centers in Alkali Halides, Academic Press, New York.

J.H. Schulman and W.D. Compton, 1962. Color Centers in Solids, MacMillan, New York.

V.L. Skinner, P.W. Levy, and J.A. Kierstead, 1982. Gamma-ray Induced Thermoluminescence of Synthetic and Natural Rock Salt. (In preparation).

A.M. Stoneham, 1975. Theory of Defects in Solids, Clarendon Press, Oxford.

K.J. Swyler, R.W. Klaffky, and P.W. Levy, 1979. Radiation Damage Studies on Synthetic NaCl Crystals and Natural Rock Salt for Waste Disposal Applications, Scientific Basis of Nuclear Waste Management, Vol. 1, G.J. McCarthy, editor (Plenum, New York), p. 349.

K.J. Swyler, R.W. Klaffky, and P.W. Levy, 1980. Recent Studies on Radiation Induced Color Centers and Colloid Formation in Synthetic NaCl and Natural Rock Salt for Waste Disposal Applications, Int. Sym. on the Sci. Basis for Nuclear Waste Management, Vol. II, C.J.M. Northrup, editor (Plenum, New York) p. 553.

K.J. Swyler, R.W. Klaffky, and P.W. Levy, 1982. Radiation Induced F-center and Colloid Formation in Melt Grown Synthetic Rock Salt between 100 and 300°C, BNL 29818, to be issued as a ONWI Topical Report.

L.J. Teutonico, 1970. Dislocations in Hexagonal Crystals, Mater. Sci. Eng. 6, 27.

APPENDIX

ON THE RELATION BETWEEN HYDROSTATIC STRESS AND DILATATIONAL STRAIN IN ANISOTROPIC ELASTIC MEDIA

In an anisotropic elastic medium, stress and strain are linearly related by a relation of the form

$$\sigma_{ij} = F_{ijkl}\,\epsilon_{kl} \qquad \text{(A1)}$$

where σ_{ij}, ϵ_{kl} represent the components of the stress and strain fields, respectively, and F_{ijkl} is the elastic constant tensor. The hydrostatic stress P, i.e. the hydrostatic pressure of the stress field, is given by

$$P = -\frac{1}{3}(\sigma_{11} + \sigma_{22} + \sigma_{33}) \,. \qquad \text{(A2)}$$

From (A1) one obtains

$$\begin{aligned}(\sigma_{11}+\sigma_{22}+\sigma_{33}) = {} & (F_{11}+F_{12}+F_{13})\epsilon_{11}+(F_{12}+F_{22}+F_{23})\epsilon_{22} \\ & +(F_{13}+F_{23}+F_{33})\epsilon_{33}+2(F_{16}+F_{26}+F_{36})\epsilon_{12} \\ & +2(F_{15}+F_{25}+F_{35})\epsilon_{13}+2(F_{14}+F_{24}+F_{34})\epsilon_{23}\end{aligned} \qquad \text{(A3)}$$

where we have used the contracted notation for the F_{ijkl} ($ij \to i$, $i = j$; $ij \to k+3$, $i \neq j$). It would appear that, in general, there is no direct relationship between the hydrostatic stress and the dilatational strain Δ, defined as the sum of the principal strains:

$$\Delta = (\epsilon_{11} + \epsilon_{22} + \epsilon_{33}) \,. \qquad \text{(A4)}$$

One must bear in mind, however, that the various F_{ij} are not independent. The general transformation formula for the elastic constant tensor in an anisotropic medium is

$$F_{ijkl} = \ell_{ip}\ell_{jq}\ell_{kr}\ell_{ls}\, c_{pqrs} \tag{A5}$$

where c_{pqrs} is the elastic constant tensor referred to the crystal axes a_i, F_{ijkl} the elastic constant tensor referred to an arbitrary Cartesian system x_i and ℓ_{kr} is the direction cosine of the x_k axis with respect to a_r.

For cubic crystals, in which there are only three independent elastic constants (c_{11}, c_{12}, c_{44}), Eq. (A5) can be written in the simple form

$$F_{ij} = \lambda_{ij} + \delta f_{ij} \tag{A6}$$

where

$$\delta = c_{11} - c_{12} - 2c_{44} \tag{A7}$$

$$\lambda_{11} = \lambda_{22} = \lambda_{33} = c_{11}$$

$$\lambda_{12} = \lambda_{23} = \lambda_{13} = c_{12} \tag{A8}$$

$$\lambda_{44} = \lambda_{55} = \lambda_{66} = c_{44}$$

and all other λ_{ij} are zero. The quantities f_{ij} are functions only of the direction cosines and are given as follows:

$$f_{11} = -2(\ell_{11}^2\ell_{12}^2 + \ell_{11}^2\ell_{13}^2 + \ell_{12}^2\ell_{13}^2) \qquad f_{22} = -2(\ell_{21}^2\ell_{22}^2 + \ell_{21}^2\ell_{23}^2 + \ell_{22}^2\ell_{23}^2)$$

$$f_{12} = f_{66} = \ell_{11}^2\ell_{21}^2 + \ell_{12}^2\ell_{22}^2 + \ell_{13}^2\ell_{23}^2 \qquad f_{23} = f_{44} = \ell_{21}^2\ell_{31}^2 + \ell_{22}^2\ell_{32}^2 + \ell_{23}^2\ell_{33}^2$$

$$f_{13} = f_{55} = \ell_{11}^2\ell_{31}^2 + \ell_{12}^2\ell_{32}^2 + \ell_{13}^2\ell_{33}^2 \qquad f_{24} = \ell_{21}^3\ell_{31} + \ell_{22}^3\ell_{32} + \ell_{23}^3\ell_{33}$$

$$f_{14} = f_{56} = \ell_{11}^2\ell_{21}\ell_{31} + \ell_{12}^2\ell_{22}\ell_{32} + \ell_{13}^2\ell_{23}\ell_{33} \qquad f_{25} = f_{46} = \ell_{21}^2\ell_{11}\ell_{31} + \ell_{22}^2\ell_{12}\ell_{32} + \ell_{23}^2\ell_{13}\ell_{33}$$

$$f_{15} = \ell_{11}^3\ell_{31} + \ell_{12}^3\ell_{32} + \ell_{13}^3\ell_{33} \qquad f_{26} = \ell_{21}^3\ell_{11} + \ell_{22}^3\ell_{12} + \ell_{23}^3\ell_{13} \qquad \text{(A9)}$$

$$f_{16} = \ell_{11}^3\ell_{21} + \ell_{12}^3\ell_{22} + \ell_{13}^3\ell_{33} \qquad f_{33} = -2(\ell_{31}^2\ell_{32}^2 + \ell_{31}^2\ell_{33}^2 + \ell_{32}^2\ell_{33}^2)$$

$$f_{34} = \ell_{31}^3\ell_{21} + \ell_{32}^3\ell_{22} + \ell_{33}^3\ell_{23} \qquad f_{35} = \ell_{31}^3\ell_{11} + \ell_{32}^3\ell_{12} + \ell_{33}^3\ell_{13}$$

$$f_{36} = f_{45} = \ell_{31}^2\ell_{11}\ell_{21} + \ell_{32}^2\ell_{12}\ell_{22} + \ell_{33}^2\ell_{13}\ell_{23} \ .$$

The above equations show that, in a cubic crystal, one always has $F_{14} = F_{56}$, $F_{25} = F_{46}$, $F_{36} = F_{45}$. With the aid of the orthogonality relations $\ell_{ij}\ell_{ik} = \delta_{jk}$ (Kronecker delta), one obtains from eqs. (A6)-(A9) that

$$F_{11} + F_{12} + F_{13} = F_{12} + F_{22} + F_{23} = F_{13} + F_{23} + F_{33} = c_{11} + 2c_{12} \qquad \text{(A10)}$$

$$F_{16} + F_{26} + F_{36} = F_{15} + F_{25} + F_{35} = F_{14} + F_{24} + F_{34} = 0 \ .$$

These results apply for any coordinate system x_i, i.e. they are independent of orientation. Hence, from eq. (A3) we see that, for any elastic field $(\sigma_{ij},\varepsilon_{ij})$ in a cubic crystal, the sum of the principal stresses is always proportional to the sum of the principal strains by

$$(\sigma_{11} + \sigma_{22} + \sigma_{33}) = (c_{11} + 2c_{12})(\varepsilon_{11} + \varepsilon_{22} + \varepsilon_{33}) \tag{A11}$$

If we define the crystal bulk modulus as

$$B = \frac{1}{3}(c_{11} + 2c_{12}) \tag{A12}$$

then we can state that, in cubic crystals, the hydrostatic stress and the dilatational strain are related by

$$P = -B\Delta. \tag{A13}$$

To see whether or not an analogous result could be expected to obtain in other crystal classes, similar calculations were carried out for hexagonal crystals for which there are five elastic constants c_{11}, c_{33}, c_{12}, c_{13}, c_{44}. Due to rotational symmetry about the c-axis the transformed elastic constants in a hexagonal crystal involve only the three direction cosines (α,β,γ) of the (x_1,x_2,x_3) axes with respect to the c-axis (Teutonico, 1970). The expression for the sum of the principal stresses in a hexagonal crystal is found to be

$$\begin{aligned}(\sigma_{11} + \sigma_{22} + \sigma_{33}) &= (c_{11} + c_{12} + c_{13})(\varepsilon_{11} + \varepsilon_{22} + \varepsilon_{33}) \\ &+ a(\alpha^2\varepsilon_{11} + \beta^2\varepsilon_{22} + \gamma^2\varepsilon_{33} + 2\alpha\beta\varepsilon_{12} + 2\alpha\gamma\varepsilon_{13} + 2\beta\gamma\varepsilon_{23})\end{aligned} \tag{A14}$$

where

$$a = (c_{33}-c_{11}) + (c_{13}-c_{12}) . \qquad \text{(A15)}$$

The quantity a would be zero only if the material is isotropic. Even for an infinitely long dislocation parallel to $x_3(\varepsilon_{33} = 0)$ the quantity in square brackets in (A14) is zero only for specific orientations. Therefore, in a hexagonal crystal, σ_{ii} is in general not proportional to ε_{ii}. It is presumed that in crystals of symmetry lower than hexagonal the same result would obtain.

Hence the result that the hydrostatic stress is always proportional to the dilatational strain appears to be unique to cubic crystals.